CHAPTER 1

NASA-Boeing Transonic Truss-Braced Wing X-66A, Sustainable Flight Demonstrator (https://www.nasa.gov/image-article/nasa-boeing-provide-a-peak-at-what-the-x-66a-will-look-like/) (Image Credit: Boeing)

Introduction: Propulsion in Sustainable Aviation

1.1 History of the Airbreathing Jet Engine, a Twentieth-Century Invention—The Beginning

Powered flight is a twentieth-century invention. The era of powered flight began on December 17, 1903, with the Wright brothers who designed, fabricated, and flew "The Flyer" in Kitty Hawk, North Carolina. The power onboard *The Flyer* was a gas powered, 12-hp reciprocating intermittent combustion engine. This type of engine, with a propeller, provided power to all (manned) aircraft until the late 1930s. The history of aircraft gas turbine engines started in January 1930 with a patent issued to Frank Whittle in Great Britain. Figure 1.1 shows a p–v diagram and components of the Whittle engine as they appeared in the patent application. The flow pattern and engine assembly are shown in Figure 1.2. The performance of the W1 engine and the aircraft that flew it are shown in Figure 1.3. An engineer at work, Sir Frank Whittle, the inventor of the jet engine, with a slide rule is shown in Figure 1.4. For more details on the Whittle turbojet, see Meher-Homji (1).

The gas turbine engine in Figure 1.1 is based on the Brayton cycle. The compression in the Whittle engine is achieved via a double-sided centrifugal compressor. The axial compressor had not been developed due to aerodynamic stability complications. The combustion takes place in a reverse-flow burner that is very large relative to other engine components. The straight throughflow burner had posed problems with stable combustion and thus a reverse-flow combustor

Aircraft Propulsion: Toward Net-Zero Aviation, Fourth Edition. Saeed Farokhi.

Companion website: www.wiley.com/go/Farokhi/Aircraft_Propulsion4e

■ **FIGURE 1.1**
Patent drawings of Sir Frank Whittle jet engine

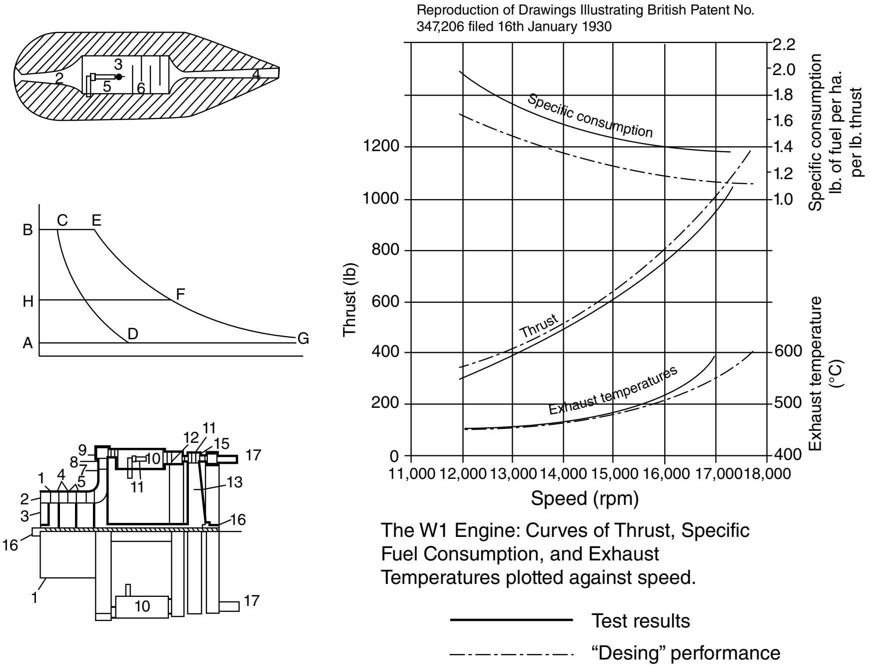

The W1 Engine: Curves of Thrust, Specific Fuel Consumption, and Exhaust Temperatures plotted against speed.

——— Test results

—·—·—·— "Desing" performance

■ **FIGURE 1.2**
The assembly and flow pattern in Whittle jet engine

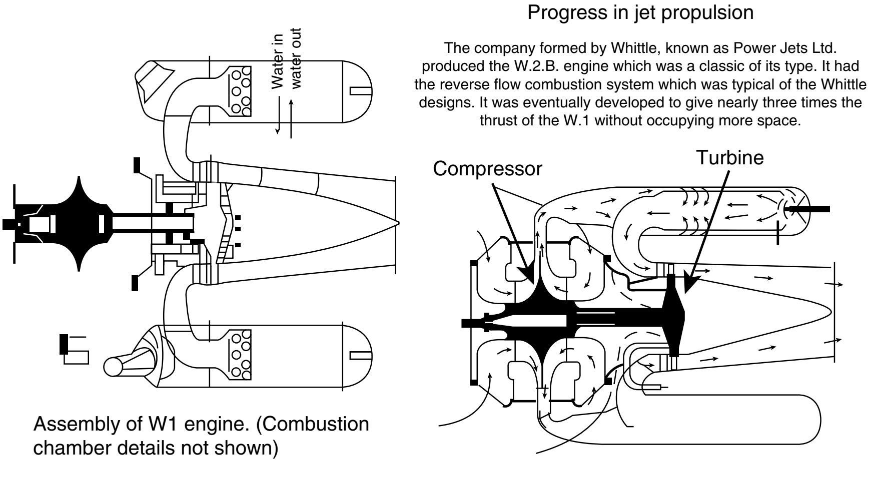

Assembly of W1 engine. (Combustion chamber details not shown)

Progress in jet propulsion

The company formed by Whittle, known as Power Jets Ltd. produced the W.2.B. engine which was a classic of its type. It had the reverse flow combustion system which was typical of the Whittle designs. It was eventually developed to give nearly three times the thrust of the W.1 without occupying more space.

■ **FIGURE 1.3**
Performance testing of Whittle jet engine, known as W1, and the experimental aircraft, Gloster E28/39, that flew it in 1941. (Source: Crown Publications)

Gloster Experimental Aeroplane E28/39 at Takeoff.
(Royal Aerospace Establishment, Crown Copyright.)

■ **FIGURE 1.4**
Sir Frank Whittle with a slide rule. (Source: Crown Publications)

FIGURE 1.5 **The first historic meeting between the two inventors of the jet engine took place in WPAFB on May 3, 1978. (Source: AFRL/AFMC)**

provided the needed flame stability in the burner. The compressor shaft power is delivered from a single-stage axial-flow turbine.

In an independent effort, Hans-Joachim Pabst von Ohain invented a turbojet engine in Germany that was granted a patent in 1936. In 1937, von Ohain's engine, designated as the He S-1 turbojet engine with hydrogen fuel, was tested and produced a thrust of 250 lb at 10,000 rpm. Von Ohain's engine was the first to be developed ahead of the Whittle engine and flew on the first jet-powered aircraft, Heinkel 178, on August 27, 1939. Both Whittle and von Ohain are credited as the coinventors of airbreathing gas turbine engines. Figure 1.5 shows the two inventors of the jet engine, a historic meeting on May 3, 1978. A recent book by Eckardt (2) gives a fascinating account of early jet development stemming from research in the United Kingdom (UK), Germany, and Switzerland. This book is highly recommended for further reading.

The first production jet aircraft was the Messerschmitt Me 262, shown in Figure 1.6. Two Jumo 004B turbojet engines powered the Messerschmitt Me 262 jet fighter. The Me 262's first flight was on July 18, 1942. Dr. Anselm Franz of the Junkers Engine Company designed the Jumo 004, which was based on von Ohain's patent. The Jumo 004B engine cutaway is shown in Figure 1.7. This engine has many modern gas turbine features such as axial-flow compressor and a straight throughflow combustor with air cooling of the turbine and the nozzle. For more details, see Meher-Homji (3).

The drawing of the Jumo 004B turbojet engine in Figure 1.7 shows an air-cooling system that bleeds air from the compressor and cools the turbine and the

FIGURE 1.6 **The first production jet aircraft, Me 262**

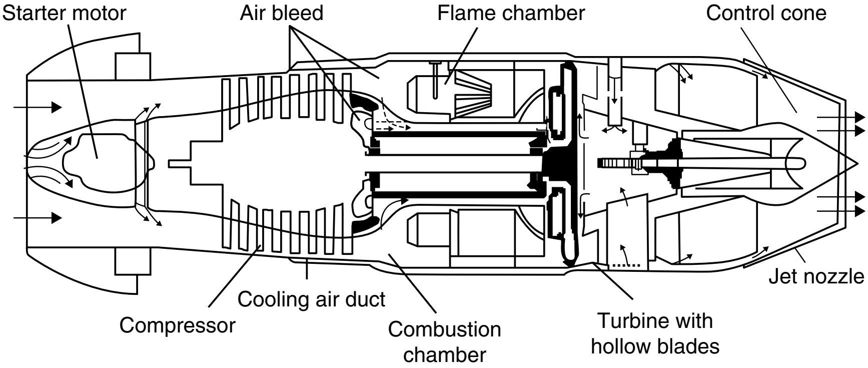

■ **FIGURE 1.7** **Jumo 004B engine cutaway features an axial-flow compressor, a straight through flow combustor, an air-cooled axial turbine, and an exhaust nozzle**

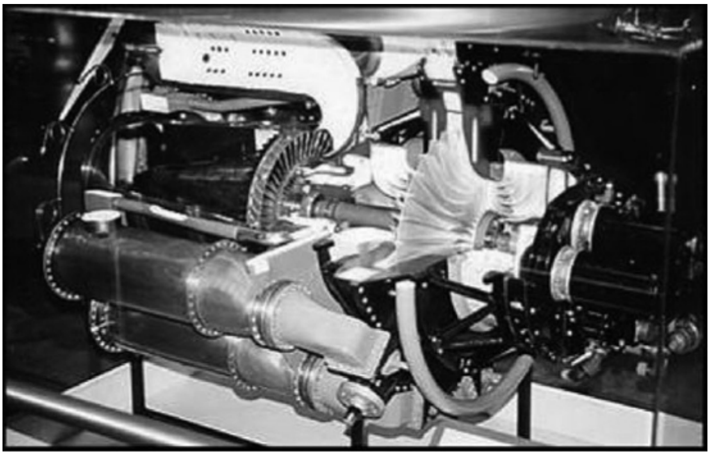

■ **FIGURE 1.8** **The first US-produced aircraft gas turbine engine. (Source: Courtesy of US Air Force Museum)**

exhaust nozzle. The engine produces ~2000 lbf of thrust at an airflow of 46.6 lbm/s. The engine pressure ratio is 3.14, turbine inlet temperature is 1427 °F, and the specific fuel consumption is 1.4 lbm/h/lbf-thrust. The engine dry weight is ~1650 lbf, and its diameter and length are ~30 and 152 in., respectively. Engine component efficiencies are reported to be 78% compressor, 95% combustor, and 79.5% turbine. We will put these numbers in perspective when we compare them with their modern counterparts.

The jet engine came from Great Britain to the United States in 1941. The J-31 (also known by its company designation, I-16) was the first turbojet engine produced in quantity in the United States. It was developed from the General Electric I-A, which was a copy of the highly secret British "Whittle" engine. Figure 1.8 shows the J-31 gas turbine engine (Courtesy of Air Force Museum).

1.2 Innovations in Aircraft Gas Turbine Engines

In this section, we introduce the most significant innovations in the gas turbine industry since the introduction of the aircraft jet engine by Whittle and von Ohain. Dawson (4) and Wallace (5) as well as the NASA websites (6, 7) and NASA publication (8) should be consulted for further information.

1.2.1 Multi-spool Configuration

To achieve a high-pressure ratio gas turbine engine, two distinct and complementary approaches were invented in the United States. One is the multi-spool concept (developed by Pratt & Whitney) and the second is the variable stator (developed by GE). The multi-spool concept combines several compressor stages together in two or three groups, known as the low-pressure compressor (LPC), intermediate-pressure compressor (IPC), and high-pressure compressor (HPC). A different shaft that spins at different rotational speeds drives each group. Figure 1.9 shows the Trent 1000, a modern Rolls-Royce engine that employs three spools.

1.2.2 Variable Stator

The need to adjust the flow direction in a multistage high-pressure ratio compressor (in starting and off-design) prompted Gerhard Neumann of GE to invent the variable stator. By allowing the stators to rotate in pitch, compressors can operate at higher pressure ratios and away from stall. Modern gas turbine engines use variable stators in their LPC and IPC. The high-temperature environment of HPC has not been hospitable to variable stators.

1.2.3 Transonic Compressor

Better understanding of supersonic flow and the development of high strength-to-weight ratio titanium alloy allowed the development of supersonic tip fan blades. The transonic fan is borne at a high shaft speed that creates a relative supersonic flow at the tip and a subsonic flow at the hub. A modern transonic fan stage produces an *average* stage pressure ratio of ~1.6. The Jumo 004B produced a cycle pressure ratio of 3.14 with eight stages, which means an average stage pressure ratio of ~1.15. Therefore, to achieve a pressure ratio of 3.14, we need only two transonic fan stages instead of eight. The higher compression per stage has allowed a reduction in engine weight, size, and part count and has improved reliability. The advances in computational fluid dynamics (CFD) and nonintrusive testing

■ FIGURE 1.9 **Three-spool gas turbine engine as developed by Rolls-Royce. (Source: The Jet Engine 2005. Reproduced by permission from The Jet Engine, Copyright Rolls-Royce plc 2005)**

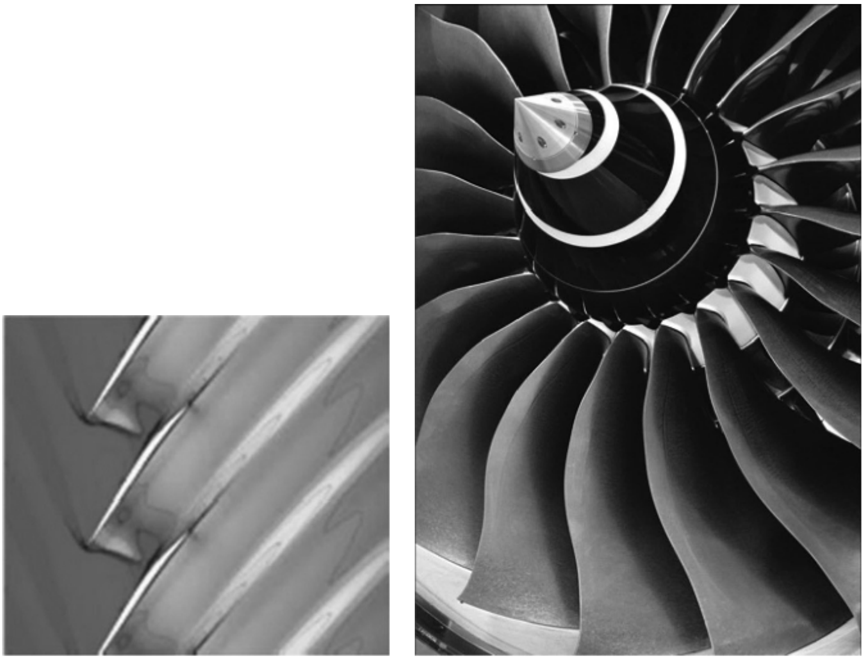

(a) (b)

■ **FIGURE 1.10** **(a) CFD in transonic compressor rotor flowfield. (Source: Courtesy of NASA); (b) advanced transonic fan. (Source: Reproduced with permission from Rolls-Royce plc)**

techniques have paved the way for a better understanding of supersonic flow in compressors. A compressor flow simulation is shown in Figure 1.10(a). The rotor passage shock, boundary layer interaction, and subsequent flow separation are clearly visualized in Figure 1.10(a). An advanced transonic fan is shown in Figure 1.10(b) from Rolls-Royce.

1.2.4 Low-Emission Combustor

The gas turbine combustor has perhaps seen the most dramatic innovations/changes since the Whittle reverse-flow burner. A better understanding of the combustion process, from atomization and vaporization of the fuel to mixing with air and chemical reactions, has allowed efficient combustion to take place in small spaces. For example, compare the relative length and volume of the combustor in GP7000, shown in Figure 1.11, to the Whittle engine or Jumo 004B.

In the textbox of Figure 1.11, we note that the combustor emissions are characterized by their nitric oxide formation, the so-called NO_x, the unburned hydrocarbon (UHC) emission, and finally carbon monoxide formation in the exhaust nozzle flow. To achieve low levels of pollutant emissions, different concepts in "staged combustion" are developed by aircraft engine manufacturers (as shown in Figure 1.12).

1.2.5 Turbine Cooling

The need to cool the turbine stems from being able to operate the combustor at higher temperature (to produce more thrust) and to achieve turbine durability, that is, an improved component life. The first production turbojet engine, Jumo 004B,

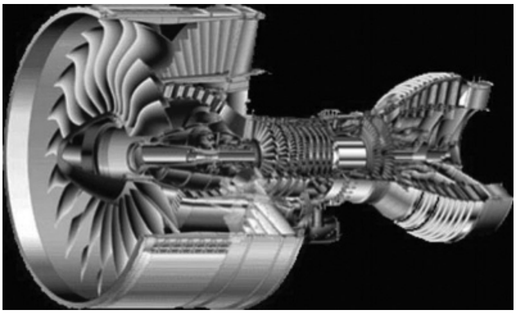

Engine alliance engine: GP7000
T.O. Thrust: 76,500 lbs/340 kN
OPR: 36^{+} (on GP7200)
BPR (cruise): 8.7
Fan diameter: 116.7 in.
Emissions:
NO_x: 59.7 g/kN
UHC: 3.9 g/kN
CO: 33.8 g/kN
Noise: 22.9 dB margin to stage 3

■ **FIGURE 1.11** **Engine Alliance engine GP7000. (Source: Reproduced with permission from the Engine Alliance). [Note: Engine Alliance is a 50/50 joint venture between GE Aviation and Pratt & Whitney.]**

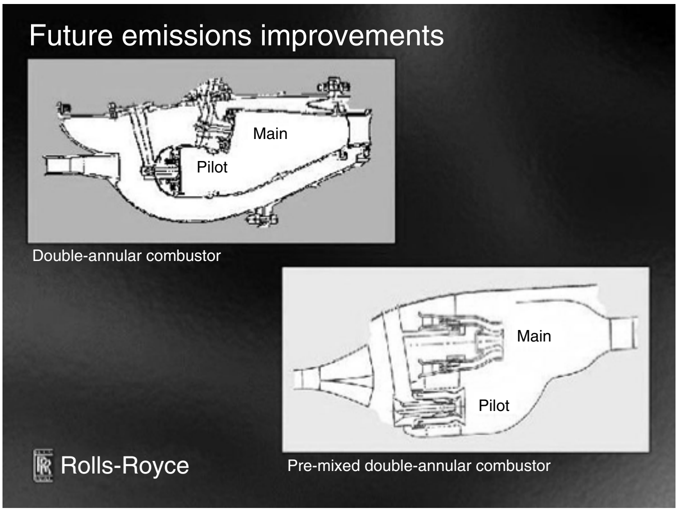

■ **FIGURE 1.12** **Concepts in low-emission combustor design. (Source: Reproduced with permission from Rolls-Royce plc)**

utilized internal cooling for the turbine blades. So, the concept is as old as the turbojet engine itself. Improved manufacturing techniques and better understanding of the flow physics involved in coolant ejection, mixing with hot gas, and three-dimensional flow in turbines have allowed for a *rationed* approach to coolant usage as well as component life enhancement. Figure 1.13 shows a single- and a multi-pass internal cooling of a turbine blade that incorporates film cooling as well as thermal protective (or barrier) coating (TPC or TBC) to reduce the heat transfer to turbine blades.

1.2.6 Exhaust Nozzles

The concept of an exhaust nozzle for aircraft jet engines has changed from a simple convergent duct that was used to propel the hot exhaust gases to a variable-geometry and multitasked component in modern designs. The new tasks involve thrust reversing, thrust vectoring, noise suppression, and dynamic stability enhancement of maneuvering aircraft. To achieve these goals, advancements in nozzle cooling, actuation, and manufacturing had to be realized. Figure 1.14 shows a sophisticated propulsion layout (and nozzle system) in F-35 aircraft that has vertical takeoff/landing (VTOL) capability as well as roll control in hover. Figure 1.15

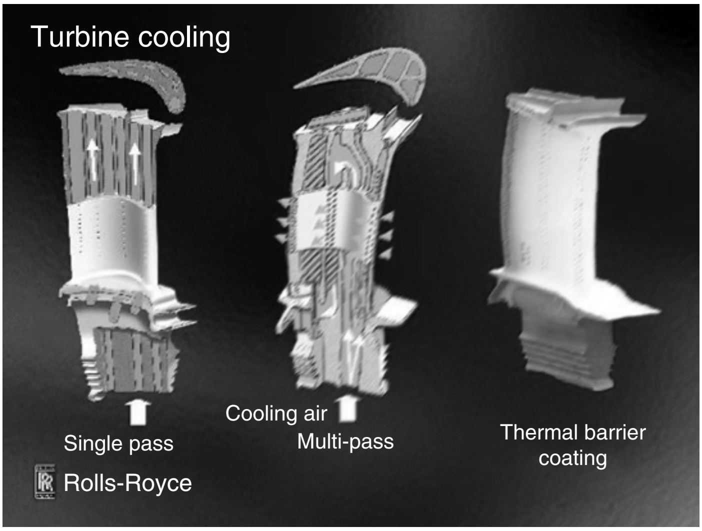

■ **FIGURE 1.13** **Turbine blade cooling. (Source: Reproduced with permission from Rolls-Royce plc)**

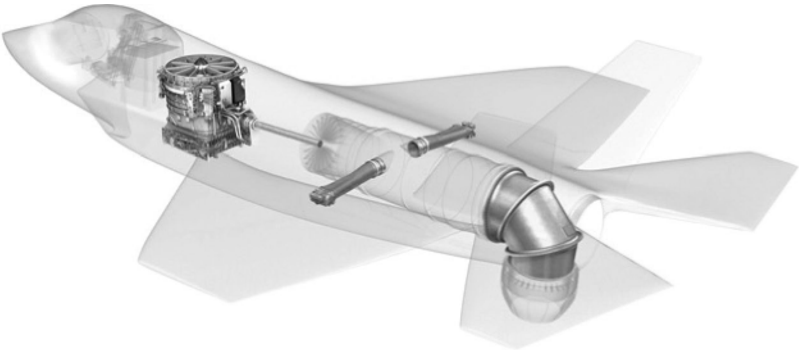

■ **FIGURE 1.14** **Propulsion layout for vertical landing and stability of an F-35 Joint Strike Fighter. (Source: Reproduced with permission from Rolls-Royce plc)**

■ **FIGURE 1.15** **F119 engine that powers F-22 Raptor is shown in vector thrust. (Source: Reproduced with permission of United Technologies Corporation, Pratt & Whitney)**

shows a ±20° vector thrust in an F119 engine developed by Pratt & Whitney for F-22 *supercruise* aircraft.

1.2.7 Modern Materials and Manufacturing Techniques

Nonmetallics and composite materials represent a sizable change in modern material usage in aircraft and jet engines. Metal matrix composites (MMCs) technology offers a high strength-to-weight ratio relative to titanium and nickel superalloys suitable for fan blades. Single crystal turbine blades offer more resistance to vibration and thus fatigue failure. Ceramic matrix composites (CMCs) can operate at high temperatures of high-pressure turbine (HPT) with reduced cooling requirement. A manufacturing technique that utilizes a honeycomb core with a composite skin offers weight and stress reductions in fan blades. Compressor weight savings are derived from bladed disk, *Blisk*, and bladed ring, *Bling*, manufacturing technology. All these are shown in Figure 1.16.

An example of a modern engine is the EJ200, which powers the "Eurofighter" Typhoon (shown in Figure 1.17). Its design features are tabulated in Table 1.1.

The modern materials and the manufacturing techniques that we have discussed are described in Table 1.1. Compare the turbine inlet temperature (T_{t4}) in the EJ200 and Jumo 004B or *thrust-to-weight ratio*.

Additive manufacturing (AM) is the new game changer in the aviation and aerospace industry. Digital files from computer-aided design/computer-aided manufacturing (CAD/CAM) are used in 3D printers to generate intricate components and prototypes for the aviation and aerospace industry, including gas turbine engines. The advancement in laser powder bed fusion and electron beam melting powder bed fusion allows for metallic parts to be manufactured in support of test rigs, engine development, engine test, or production (9). The choice of materials, precision (e.g. nano printing), and composite tooling has revolutionized industrial manufacturing and rapid prototyping in aviation. For example, GE Aerospace *LEAP engine* uses 19 3D-printed fuel nozzles in its turbofan engines, which results in 15% fuel efficiency improvement (according to company reports).

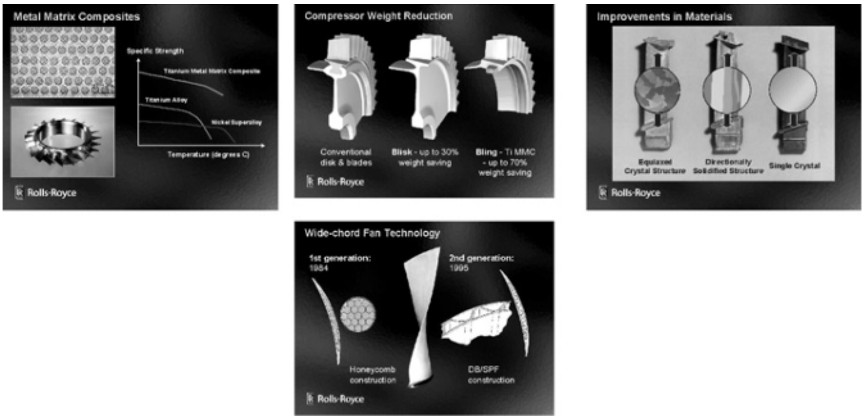

■ FIGURE 1.16 Advanced materials and manufacturing techniques. (Source: Reproduced with permission from Rolls-Royce plc)

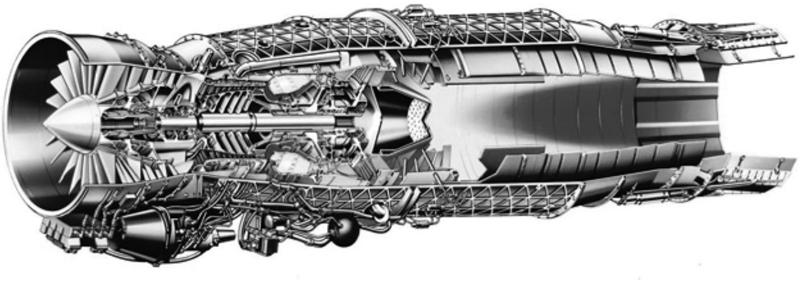

■ FIGURE 1.17 Cutaway of EJ200, an afterburning turbofan engine designed for the Eurofighter. (Source: Reproduced with permission from Rolls-Royce plc)

■ **TABLE 1.1**
EJ200 specifications

		Fan/compressor stages	1/3/5
		LPT/HPT	1/1
		Max. diameter	29 in.
Two-spool configuration		OPR	26:1
Fan technology		BPR	0.4
Wide chord		Length	157 in.
Single crystal *Blisk* (bladed disk)		Dry weight	2286 lbf
No IGV		Sfc (max. power)	0.81 lbm/h/lbf
Three-stage LPC:	4.2 PR	Sfc w. AB	1.75 lbm/h/lbf
Mass flow:	77 kg/s or 170 lbm/s	Thrust (SL)	13,500 lbf
HPC:	Single crystal *Blisk*	Thrust w. AB	20,250–22,250 lbf
T_{t4}:	1800 K (or 2780 °F)	Thrust/weight (Dry)	5.92
HPT:	Air cooled + TPC (two-layers)	Thrust/weight (AB)	9.1
C–D nozzle:	Titanium alloy	Thrust vectoring:	23° any direction
		Engine management	FADEC + monitoring unit

A new milestone in 3D-printed jet engine is reported in June/July 2024 Mechanical Engineering Magazine. The Beehive Industries reported the first *fire test* of a demonstration jet engine in March 2024 that was almost entirely made up of 3D-printed components. The demonstration engine, BJT-500, is in a class of engines that produces 250–1000 lb of thrust (see Mechanical Engineering Magazine (June/July 2024) and Beehive Industries website (https://www.beehive-industries.com)).

The use of AM in space has brought 3D printing capability onboard the International Space Station (ISS). The experience gained on the ISS will be invaluable for long-term manufacturing goals on the Moon and human habitats on Mars. Conner et al. (10) give an introductory discussion on AM business products and services. For AM on the ISS, see the website of *Made in Space*. National Institute of Standards and Technology (NIST) publications may be consulted for the latest in AM technology. For more information on radiation-resistant 3D-printed materials intended for lunar missions, see Stratasys website (https://www.stratasys.com).

1.3 Twenty-First-Century Aviation Goal: *Sustainability*

Sustainability in the context of aviation is based on three inter-related concepts: the impact of aviation on the environment (i.e. climate, air quality, and noise), the renewability of the energy sources, and the societal factors (e.g. economics) that increase our need for air transportation. We begin with the element of sustainability first. Aviation impact on the environment starts at the ground level with *air quality* near airports and rises through the Earth's atmosphere with *greenhouse gas (GHG) emissions* that cause climate change. Aircraft engine emissions and noise impact air quality and health hazards at the community level. In addition to aircraft engines, auxiliary power units (APUs), the ground support equipment, ground access vehicles, construction activities, electric powerplants, and maintenance operations are also deemed to be emission sources that contribute to aviation-related environmental pollution at airports.

At the cruise altitude, GHGs, mainly carbon dioxide, (CO_2), in the engine emissions contribute to climate change through global warming effect. The impact of engine emissions on the climate in the form of nitrogen oxides (NO_x) threatens to deplete ozone in the protective ozone layer in the Earth's atmosphere and to generate harmful ozone at the ground/community level. The formation and spreading of persistent contrails in high-flying jets is the source of *aviation-induced cloudiness* (AIC), akin to naturally occurring cirrus clouds, which covers about 30% of the Earth. AIC alters radiative forcing (RF) in the upper atmosphere and thus another concern for climate change is born. In this section, we briefly address the aviation-related pollution and the magnitude of these *anthropogenic*, that is, caused by human activities, emissions on the local and the global scale.

Aviation noise generated in takeoff, climb, flyover, approach, and landing is also critical to sustainable aviation and will be addressed. The sonic boom and its alteration to a *sonic thump* that enables supersonic cruise over land are presented in Chapters 1 and 10 on supersonic and hypersonic propulsion. For additional discussions on sustainable aviation, see Farokhi (11).

1.3.1 Combustion Emissions

The combustion of fossil fuel in the air results in water vapor (H_2O) and carbon dioxide (CO_2) formations that belong to the category of GHGs. Incomplete combustion results in carbon monoxide (CO) and unburned hydrocarbon (UHC) in the exhaust jet. Nitrogen oxides, labeled as NO_x, are major concerns due to their impact on air quality. NO_x also plays a catalytic role in ozone production or depletion in the lower and upper atmosphere, respectively. The sulfur content of a fuel is dictated by the aviation (fossil) fuel production (or the refinery) process and its oxides, labeled as SO_x (mainly SO_2), contribute to local air quality concerns. Finally, particulate matter (PM) in the exhaust, known as soot and volatile gases, are combustion emissions that have condensed to solid (particle) phase, which adversely impact air quality. The US Environmental Protection Agency (EPA) has been charged with setting the emission standards for aircraft engines operated in the United States. There are two areas of concern with air pollution. The first deals with the engine emissions near airports in the landing-takeoff cycle (LTO), below 3000 ft. The second area of concern examines the effect of engine emissions at the climb-cruise-descent (CCD) phase, above 3000 ft. Figure 1.18 shows the type and nature of the emissions related

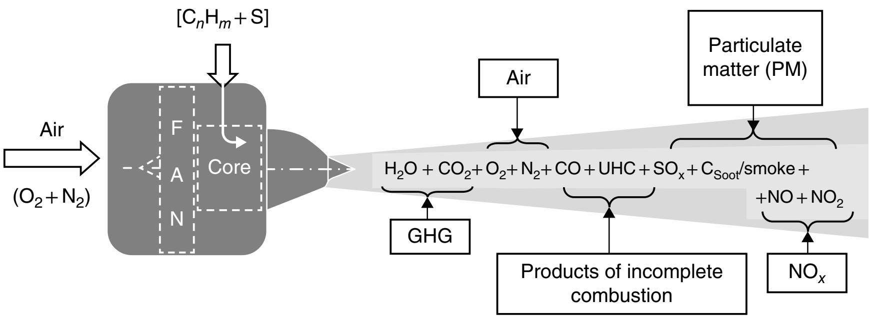

■ FIGURE 1.18 ***Tank-to-wake*** **products from the combustion of fossil fuel in an aircraft turbofan engine. (Source: Farokhi (11). Reproduced with permission of John Wiley & Sons)**

to the combustion of fossil fuels (that contain carbon) in aircraft engines, which is known as Tank-to-Wake (TTWa) in *lifecycle* analysis terminology of GHG emissions' impact on climate. The other element of lifecycle analysis accounts for the Well-to-Tank portion that contributes to GHG emissions.

1.3.2 Greenhouse Gases

Solar radiation powers our climate system on Earth. There are certain gases in the Earth's atmosphere that absorb and re-emit infrared radiation and contribute to the Earth's warmer climate. These are called GHGs. The average temperature on the Earth's surface is 298 K, whereas without the GHGs in the atmosphere it would be 255 K (i.e. 43 °C colder). The greenhouses gases in the atmosphere are composed of:

1. Carbon dioxide, CO_2
2. Water vapor, H_2O
3. Methane, CH_4
4. Nitrous oxide, N_2O

$$\left.\begin{array}{l}\textbf{5}.\ \text{Hydrofluorocarbons, HFCs}\\ \textbf{6}.\ \text{Perfluorocarbons, PFCs}\\ \textbf{7}.\ \text{Sulfur hexafluoride, SF}_6\end{array}\right\}\text{Fluorinated gases}$$

Aviation impacts the first four categories whereas the last three, fluorinated gases, are highly regulated and their impact is minimized. Carbon dioxide (CO_2) and water vapor (H_2O) dominate the list and constitute the products of complete combustion of fossil fuels in airbreathing jet engines. Note that CO_2 and H_2O are direct results of the combustion of a fuel with a molecular structure composed of carbon and hydrogen atoms, namely *hydrocarbon fuels*. The large deposit of these products in the atmosphere by a growing fleet of commercial aircraft contributes to global warming through the greenhouse effect. Once created, GHGs linger in the atmosphere, i.e. they have a lifespan of several decades, even centuries in the atmosphere before their absorption by the oceans, forests, plants, and soil.

In addition to the dynamics of the GHG in the atmosphere, there is surface *reflectance* of sunlight from ice sheets, soil, forests, and oceans, known as the *albedo effect*, that ranges from 10% to 90%. Melting ice sheets and deforestation contribute to global warming through the albedo effect. An example in the Arctic is the Greenland ice sheet albedo that showed a 5% reduction in reflectivity from 2000 to 2010 and has resulted in an accelerated melting rate of 6600 square miles of ice sheets *per year*.

Figure 1.19 shows the September 2023 sea ice extent in the Arctic (from NOAA Climate.gov). Note the comparison to 1981–2010 sea ice areal extent. The significant reduction in the sea ice areal extent is evident and indeed the scale of the problem is measured in *millions of square miles* (12).

The adverse impact of the anthropogenic GHGs in the atmosphere is universally acknowledged, but there are still a few doubts about certain conclusions. The *undeniable* fact of human impact on the atmosphere is, however, based on

■ FIGURE 1.19 **September ice sheet extent and comparison to 1981–2010 in the Arctic (September 19, 2023). (Source: NOAA Climate.gov Data: NSIDC. https://www.climate.gov/media/15597)**

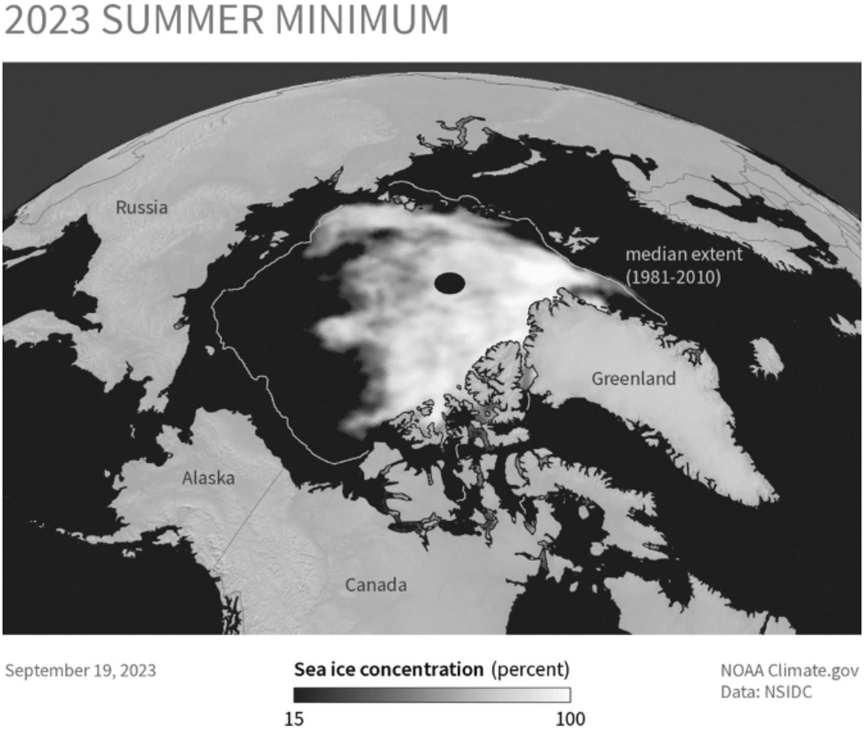

■ FIGURE 1.20 **Global atmospheric carbon dioxide from industrial revolution to 2022. (Source: Adapted from NOAA Climate.gov, March 2023; Data: NOAA, ETHZ, Our World in Data)**

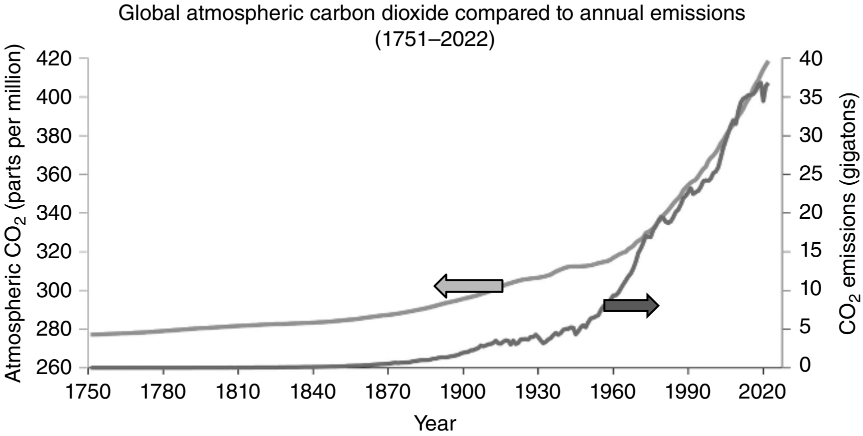

data, that is, scientific measurements. Figure 1.20 shows the carbon dioxide concentration in *parts per million* (ppm) as well as (total) carbon dioxide emissions in *Gigatons* since the Industrial Revolution 1750. It shows the rapid rise in carbon dioxide concentration in the past 272 years. The main causes are found in the increasing consumption of fossil fuels for electric power generation, home heating, and transportation. At present, there is no emission regulation for carbon dioxide and water vapor and thus no Federal Aviation Administration (FAA) engine certification requirements.

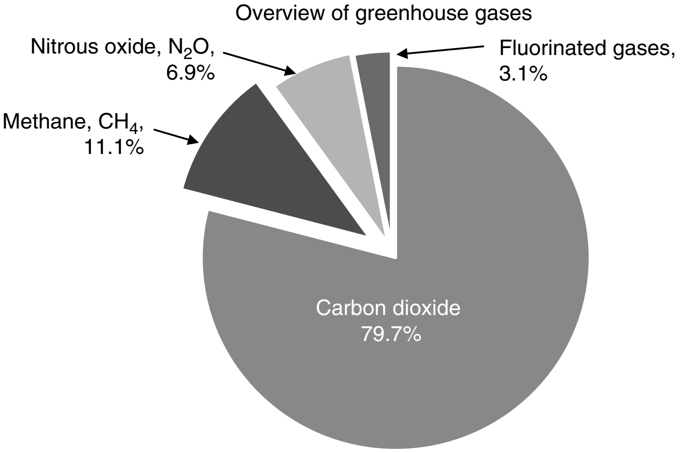

■ **FIGURE 1.21**
The inventory of GHG emissions in the United States (in 2022). (Source: Data from EPA 2022 report)

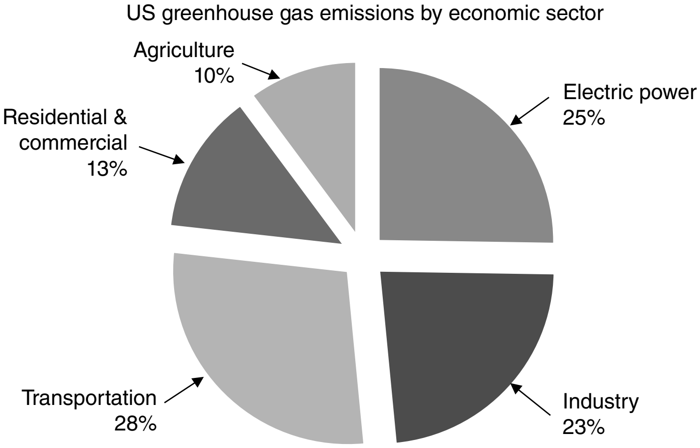

■ **FIGURE 1.22**
US GHG emissions by economic sector (2022). (Source: Data from EPA 2022 report)

Figure 1.21 shows the GHG emissions inventory in the United States in 2022. Carbon dioxide is the largest source with ~80% share in GHG emissions. Figure 1.22 shows the GHG emissions *by economic sector* in 2022. The transportation sector (i.e. road transport, rail, aviation, and shipping) contributes 28% to GHG emissions in the United States. Aviation is responsible for 12% of CO_2 emissions from all transport sources. The aviation contribution within the transport sector in the European Union is 12.4% (see European Commission (13)). In another study, Lee et al. (14) estimated the impact of aviation on climate to be around 5% of all anthropogenic effects in 2005. However, aviation is the fastest growing sector within transportation and is thus a prime candidate for a revolutionary new approach to its propulsion system, airframe design, system integration, and eco-friendly operational measures, for example, flight altitude, cruise Mach number, and air traffic management.

1.3.3 Fuels for Sustainable Aviation

Sustainable aviation demands renewable jet fuels for future air travel and an environmentally friendly replacement for the current fleet of fossil fuel-burning aircraft. Sustainable aviation also demands reliability in fuel supply and stability in fuel prices. The history of crude oil price fluctuation alone makes it an unreliable and unsustainable fuel. The price of crude oil per barrel on the world market has seen a nearly 10-fold variation in the 10 years (2008–2017), that is, crude oil was sold between ~\$15 and ~\$145 in that decade! This wild swing in crude oil prices, in a relatively short time span, is the textbook definition of fuel *price volatility*. In short, fossil fuels are not renewable, lack supply reliability, lack stability in price, and lack the requisite longevity that transportation and power industry need. On the pollution side, the combustion of fossil fuels in powerplants, aircraft engines, ships, and road vehicles produces GHG emissions, destroys ozone in the upper atmosphere, and creates harmful effects for humans through surface air quality. Moreover, GHG emissions alter radiative forcing in the upper atmosphere and contribute to climate change through rising temperatures on the Earth. In contrast, *Sustainable Aviation Fuels* (SAFs) are renewable and can help reduce GHG emissions, as well as soot and particulate matter (PM) emissions from jet engines. In addition, the absence of aromatic hydrocarbons and (oxides of) sulfur in SAF, as compared to conventional fossil fuels, is considered a significant environmental advantage of SAF, which positively impacts surface air quality. Ultimately, it is in the reduced lifecycle emissions assessment of alternative jet fuels, as compared to the conventional fossil fuels, that SAF finds strong support in the aviation industry today. Cryogenic fuels, such as liquid hydrogen (LH_2) and liquefied natural gas (LNG), which is by and large methane, are also in competition with fossil fuels and SAF. We address SAF and cryogenic fuels in Chapters 3 on cycle analysis and 5 on combustion chambers and afterburners.

For a detailed exposition and assessment of the twenty-first-century needs for the aero-propulsion industry, see Sehra and Shin (15), Epstein (16), and Farokhi (11).

1.3.4 Emerging Technologies in Sustainable Manufacturing

In a recent article in SAE International *Tech Briefs* (January 2024), five emerging technologies in manufacturing are identified and highlighted. These transformative technologies are:

1. Artificial intelligence (AI)
2. 6G connectivity
3. Digital twins (DT)
4. Extended reality (XR)
5. Sustainable manufacturing

On the AI front, cloud-connected data and AI are identified as the engines for higher productivity (see Hooper, S. article). On the promise of 6G connectivity, that is, speed and bandwidth, it is deemed as the cornerstone of AI, machine learning (ML), and DT's technologies that are envisioned as the future of manufacturing (see Kauffman, R. article). The concept of DT is not new, but beyond DT lies the potential of *interconnected digital twins* (IDT), that couples DTs in a dynamic environment that is a powerful and transformative tool (see the article by Klotz, W.). XR is envisioned as the organic evolution of virtual reality (VR), augmented reality (AR), and mixed reality (MR). These tools will be the cornerstone of industrial training and skill development, among other benefits related to industrial efficiency and collaboration (see the article by Worth, J.). On the heels of *Net-Zero Carbon Emissions* initiative, sustainable manufacturing invests in digitization, DT, and enterprise-wide energy management, throughout its supply chain. Sustainable manufacturing holds the promise of achieving the same production outcomes more efficiently, with reduced energy, less waste, and reduced carbon footprint (for more details, read Devola, E.).

1.4 New Engine Concepts in Sustainable Aviation

In this section, we first examine a few modern concepts in gas-turbine-based aircraft propulsion. The first one is the advanced turboprop (ATP) and its modern version: counter-rotating open rotor (CROR) configuration, followed by the geared turbofan (GTF) engine. Other exciting new engines are adaptive cycle engines, and an airbreathing rocket, the single stage to orbit (SSTO) engine that is under promising development in the United Kingdom. The next two concepts, wave rotor and pulse detonation engine, harness unsteadiness as a means of thrust production. The fifth is the triumph of micro-electromechanical (MEM) device manufacturing. Finally, combined cycles and modern concepts in hybrid-electric and distributed electric propulsion are briefly introduced.

1.4.1 Advanced GT Concepts: ATP/CROR and GTF

Conventional propellers lose their thrust production capability when their tip operates in supersonic flow and stalls. In the United States, Pratt & Whitney/ Allison Gas Turbine, GE Aviation, and NASA collaborated in developing the technology of advanced turboprop, *ATP*, engines in the 1970s and 1980s. These engines are generally called Propfan, while GE's gearless, direct-drive ATP is called the *Unducted Fan* (UDF). The advanced propellers operate with relative supersonic tip Mach number ($M_T \sim 1.1–1.15$) without stalling! With increasing capability in relative tip Mach number of the propeller, the cruise flight Mach number is increased to $M_0 \sim 0.8–0.82$. Several configurations in co- and counterrotating propeller sets and pusher versus tractor configurations were developed and tested. The advanced propellers are highly swept at the tip (between 30° and 40°) to improve tip aerodynamic efficiency at high relative Mach numbers. Figure 1.23 shows an early development of ATP (from GE and NASA) and a modern CROR concept from Safran Aircraft Engines. The unsteady interaction between the wake of a pylon and pusher propeller has been investigated by Farokhi (17) and is recommended for review.

The technology of the ultra-high bypass (UHB) turbofan engine developed at Pratt & Whitney utilizes an advanced gear system that improves low-pressure spool operating efficiency. The fan pressure ratio in UHB engines is reduced to accommodate bypass ratios of 12^+, which improves propulsive efficiency, cuts down on fuel consumption, and reduces jet noise and engine emissions. The first single-aisle transport aircraft equipped with GTF entered service in 2013. The engine architecture is readily scalable to include widebody aircraft thrust levels as well. Figure 1.24 shows the cutaway of the P&W GTF engine, that is, the PW1000G GTF engine family. The advanced fan gear system on the low-pressure spool is visible in Figure 1.24 (trimetric view).

■ **FIGURE 1.23**
Advanced turboprop engines

(a) GE Unducted Fan (UDF) or GE-36. (Source: Reproduced with permission from General Electric Company)

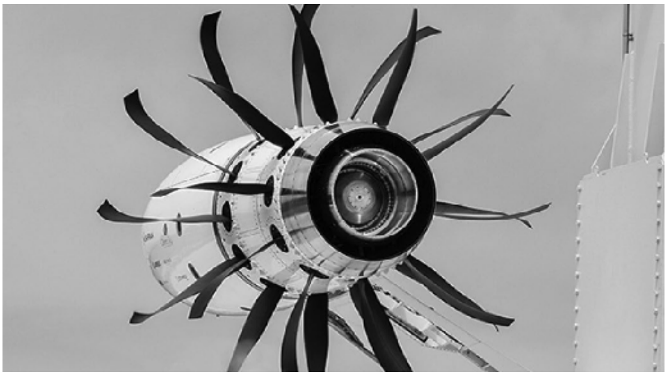

(b) Counter-rotating open rotor (CROR) engine architecture with bypass ratio in 30^+ range features 12 front and 10 aft rotor blades, 4 m diameter and 100-kN (22,000 lbf) thrust @ takeoff (SSL) (Safran Aircraft Engines)

■ **FIGURE 1.24**
Cutaway view of the PW1000G UHB-geared turbofan engine. (Source: Reproduced by permission of United Technologies Corporation, Pratt & Whitney)

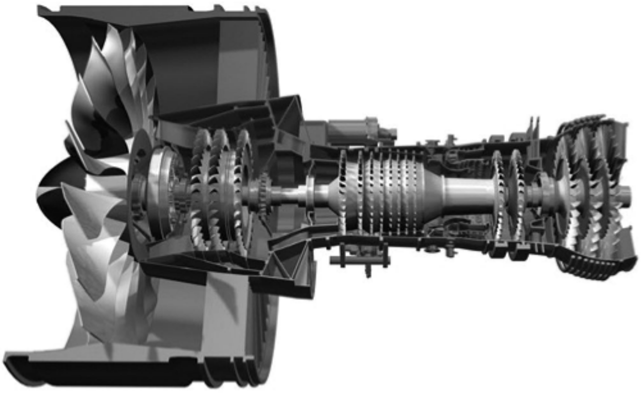

1.4.2 Advanced Airbreathing Rocket Technology

An ultra-lightweight precooler heat exchanger uses a closed-cycle helium loop to cool the air from 1000 to −150 °C in a fraction of a second (in 10 ms). This innovative counterflow precooler/heat exchanger technology is at the heart of an innovative airbreathing rocket engine that is capable of horizontal takeoff, climb, acceleration to Mach 5^+ using subcooled air in its rocket engines and then transition to pure rocket mode above 20^+ km altitude. The air intake system uses a translating cone that completely closes the inlet in pure rocket mode. Due to its versatility, this combined cycle engine is dubbed *SABRE*—Synergetic Air Breathing Rocket Engine—and is being developed by Reaction Engines Ltd. in the United Kingdom (Figure 1.25). At the time of writing, the critical components of SABRE are undergoing testing and with promising results.

The reusable SSTO winged aerospace plane that is designed around SABRE technology is in its early development phase; it is called SKYLON. The configuration of this vehicle is shown in Figure 1.26. Extensive technical information on SABRE and SKYLON can be found on the Reaction Engines Ltd. website.

1.4.3 Wave Rotor Topping Cycle

Wave rotor creates a pressure gain in the combustor, instead of the baseline pressure drop, thereby enhancing cycle efficiency. As a simple example of a higher efficiency cycle that takes advantage of constant-volume combustion, we may examine the Humphrey cycle. Schematics of the wave rotor topping cycle concept, a wave rotor hardware, and a test rig at NASA-Glenn Research Center are shown in Figure 1.27. A performance chart of the wave rotor topping cycle for small turboshaft engines, also in Figure 1.27, shows nearly 10% fuel savings compared with a baseline engine.

1.4.3.1 Humphrey Cycle Versus Brayton Cycle. An ideal Humphrey cycle is shown in Figure 1.28. Combustion takes place at constant volume in a

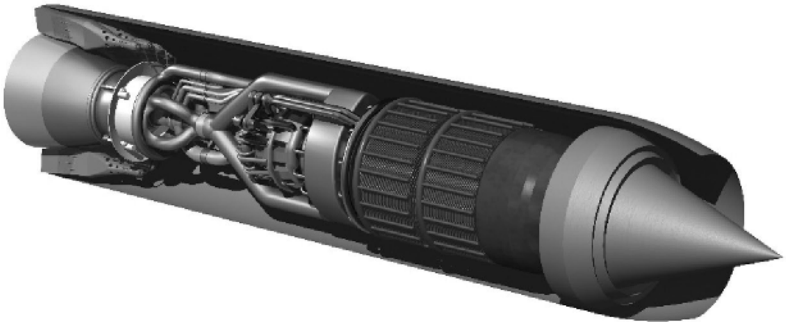

■ **FIGURE 1.25** **Cutaway of SABRE shows the heat exchanger integrated in the air intake system. (Source: Reproduced by permission of Reaction Engines Ltd.)**

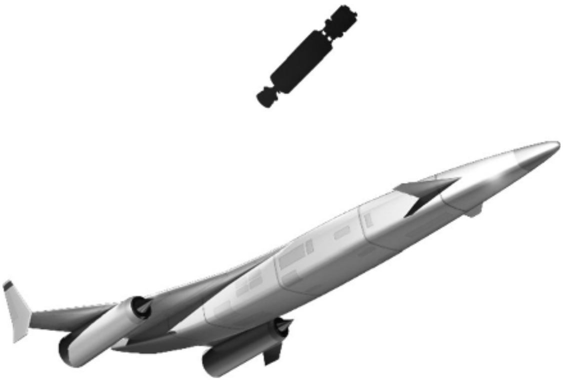

■ **FIGURE 1.26** **SKYLON in low-Earth orbit with payload separation. (Source: Reproduced by permission of Reaction Engines Ltd.)**

■ FIGURE 1.27 Schematics of the wave rotor topping cycle, hardware, and a test rig at NASA. (Source: NASA/ Public Domain)

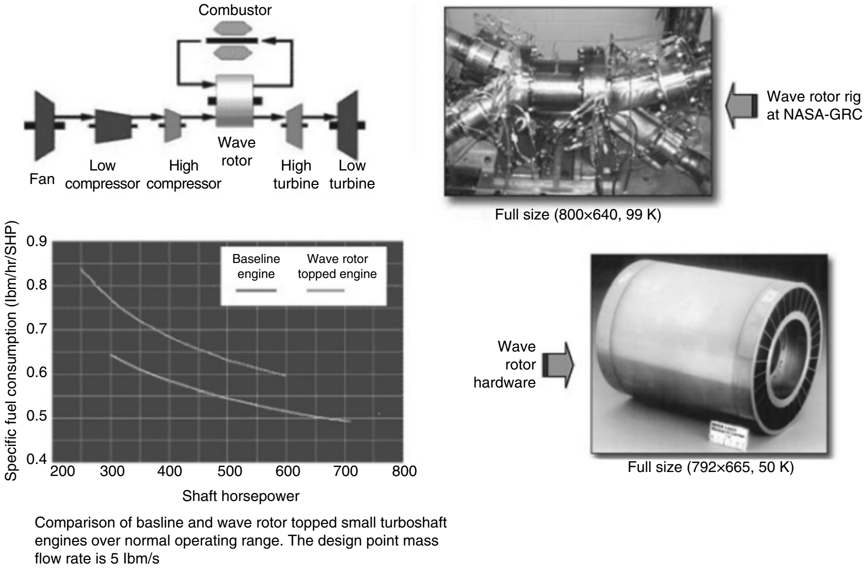

Comparison of basline and wave rotor topped small turboshaft engines over normal operating range. The design point mass flow rate is 5 lbm/s

■ FIGURE 1.28 Constant-volume and constant-pressure combustion cycles

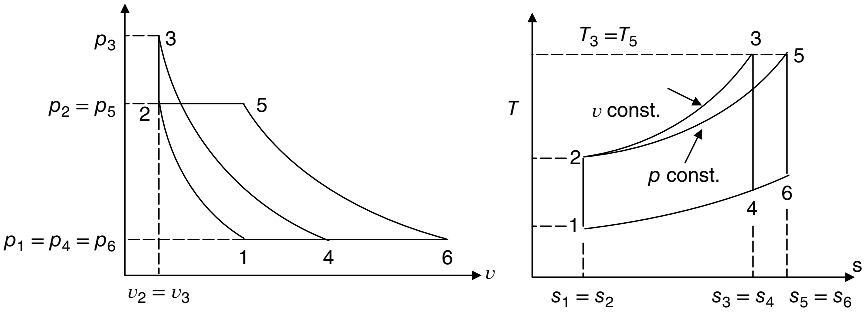

Humphrey cycle, whereas it takes place at constant pressure in an ideal Brayton cycle. We utilize the definition of cycle efficiency and thermodynamic principles to get Brayton and Humphrey cycle efficiencies.

The ideal cycle thermal efficiency of a constant-pressure combustion (Brayton) cycle: 1–2–5–6–1, is:

$$\eta_{\text{th}} = 1 - \frac{T_1}{T_2} \tag{1.1}$$

The ideal cycle thermal efficiency of a constant-volume combustion (Humphrey cycle: 1–2–3–4–1) is:

$$\eta_{\text{th}} = \frac{1 - \gamma \dfrac{T_1}{T_2}\left[\left(\dfrac{T_3}{T_2}\right)^{\frac{1}{\gamma}} - 1\right]}{\left[\dfrac{T_3}{T_2} - 1\right]} \tag{1.2}$$

where γ is the ratio of specific heats.

Cycle efficiency in the Humphrey cycle depends on T_1/T_2 and on the temperature ratio T_3/T_2 (in effect p_3/p_2). Figure 1.29 shows the ideal cycle thermal

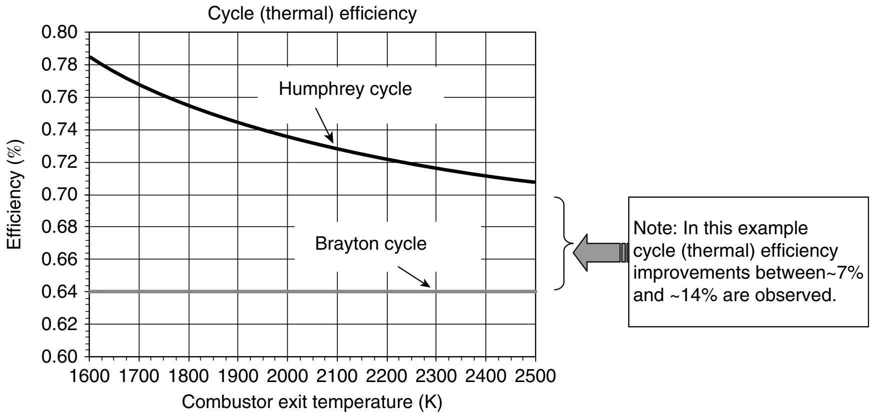

■ FIGURE 1.29 Ideal thermal efficiency of Humphrey and Brayton cycles for $\gamma = 1.4$, $T_1 = 288$ K, and $T_2 = 800$ K, with T_3 that varies between 1600 and 2500 K

Note: In this example cycle (thermal) efficiency improvements between~7% and ~14% are observed.

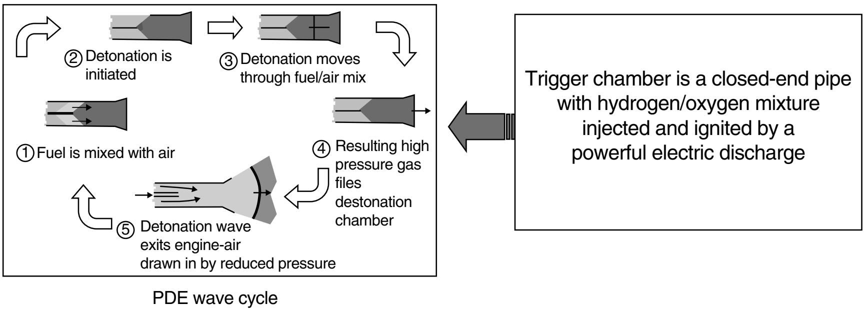

■ FIGURE 1.30 The pulse detonation engine with a trigger chamber. (Source: NASA/Public Domain)

Trigger chamber is a closed-end pipe with hydrogen/oxygen mixture injected and ignited by a powerful electric discharge

efficiency of a Brayton and a Humphrey cycle for T_1 = 288 K, T_2 = 800 K, and T_3 that varies between 1600 and 2500 K, for $\gamma = 1.4$.

Note: In this example, cycle (thermal) efficiency improvements between ~7% and ~14% are observed. For more details, see Welch et al (18) and Akbari (19, 20).

1.4.4 Pulse Detonation Engine (PDE)

The PDE is a constant-volume combustion ramjet that can produce static thrust. The operation of a PDE is like a pulsejet except combustion in a pulsejet is based on the principle of deflagration that is a *slow wave front* with a low-pressure ratio. The PDE creates a detonation wave, which is akin to an explosion that creates high-pressure shock waves. To get a feel for how often these *explosions* occur, we note the frequency of these explosions that is ~60 detonations/s. The PDE wave cycle is shown in Figure 1.30. For more discussions, see Farokhi (11).

1.4.5 Millimeter-Scale Gas Turbine Engines: Triumph of Micro-Electro-Mechanical Systems and Digital Fabrication

Microchip manufacturing techniques and some vivid imaginations have given birth to millimeter-scale gas turbine engines. Figure 1.31 shows a "button" size gas turbine engine that is designed, manufactured, and tested at MIT. At these scales, the rotor must spin at ~1,000,000 rpm to achieve the needed compression

FIGURE 1.31 Millimeter-scale gas turbine engine with the rotor and external shell. (Source: Courtesy of MIT Gas Turbine Laboratory)

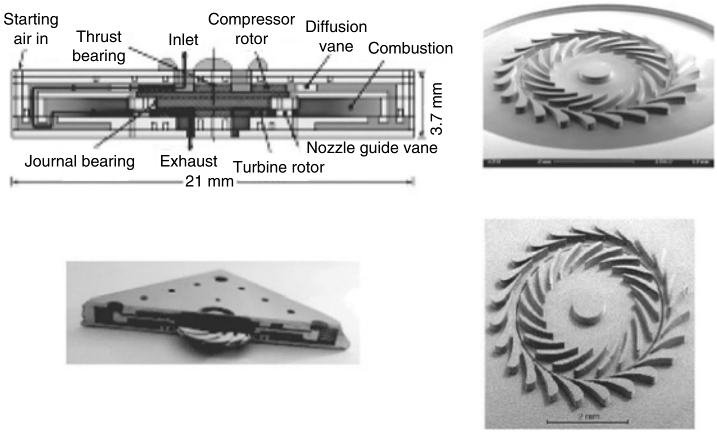

for the cycle. The process of fuel injection, atomization, vaporization, and combustion is a challenge among the myriad of other mechanical challenges in the manufacturing of millimeter-scale gas turbine engines.

1.4.6 Combined Cycle Propulsion: Engines from Takeoff to Space

We have examined the SABRE technology in SSTO in Section 1.4.3. In this section, we examine other concepts in SSTO propulsion systems. There are several developments that address combined cycles as a means of producing efficient propulsion over a wide range of flight speeds, typically from takeoff to hypersonic Mach numbers. An example of this approach is found in the airbreathing rocket engine, which is a rocket-based combined cycle (RBCC) engine. At takeoff, where conventional ramjets are incapable of producing thrust, a rocket is fired (with an ejector nozzle configuration to get a thrust boost) that accelerates the vehicle to, say, Mach 2. At Mach 2, the rocket is turned off and air intakes are opened to start a subsonic ramjet engine operation. The airbreathing engine switches from the subsonic to supersonic combustion ramjet (scramjet) near Mach 5. The scramjet will accelerate the vehicle to, say, Mach 15. The air intakes close at Mach 15 and rocket operation resumes accelerating the vehicle to orbital speeds (~Mach 25 or higher). The rocket with the ejector nozzle and computational results of Mach contours are shown in Figure 1.32. An RBCC engine can reduce launch costs by two orders of magnitude. An artist's concept of the vehicle is shown in Figure 1.33. An RBCC flightweight engine system test was conducted in 2006. Figure 1.34 shows the test firing of the airbreathing rocket.

1.4.7 Hybrid-Electric and Distributed Electric Propulsion

Implicit in greener aviation are reduced emissions that point in the direction of electrification of the aircraft propulsion and power systems. In the hierarchy of electric propulsion, we start with a hybrid propulsion and power system, which is the aviation version of the hybrid engines in automobiles. The schematic diagram of this type of propulsion system is shown in Figure 1.35 (21, 22). The propulsor is a low-pressure ratio ducted fan. Note that there are two sources of energy to the

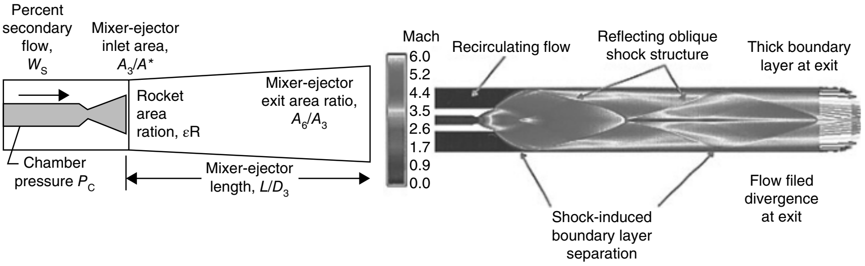

■ FIGURE 1.32 **An RBCC air-augmented rocket with an ejector nozzle (with Mach contours computed). (Source: NASA/Public Domain)**

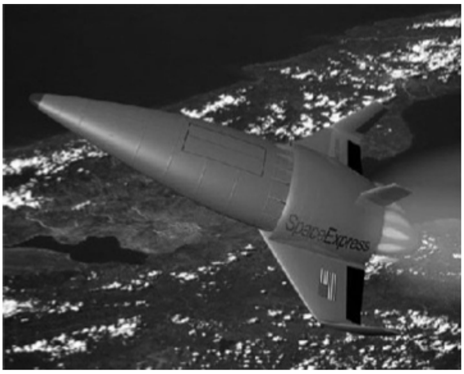

■ FIGURE 1.33 **Artist's drawing of an advanced launch vehicle using RBCC propulsion. (Source: Courtesy of NASA)**

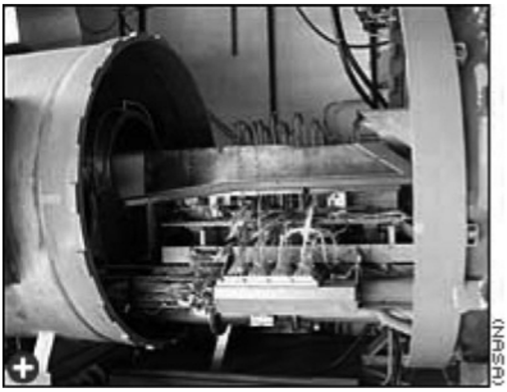

■ FIGURE 1.34 **Testing of an airbreathing rocket at NASA. (Source: Courtesy of NASA)**

propulsor: one is the jet fuel for the gas turbine engine, and the second one is the battery or electric energy storage system, such as a *capacitor*. The transmission lines are the electrical wirings that may use the ambient temperature conventional wiring, or they may use *cryogenic wiring* for high-temperature superconducting (HTS) transmission lines (21, 22). The electric fan uses a 3-phase (3φ) AC motor, as shown in Figure 1.35.

Since in hybrid propulsion the exhaust energy in the gas turbine is used to generate electricity, the hybrid-electric propulsion system produces lower atmospheric heat release than the conventional turbofan engines. Also implicit in "GREENER AVIATION" are reduced noise levels during landing-takeoff (LTO) cycle. The lower pressure ratio (PR) fans are quieter than their higher-PR counterparts. In

■ **FIGURE 1.35** **Schematic drawing of two hybrid-electric propulsion system architectures. (Source: Farokhi (11). Reproduced with permission of John Wiley & Sons)**

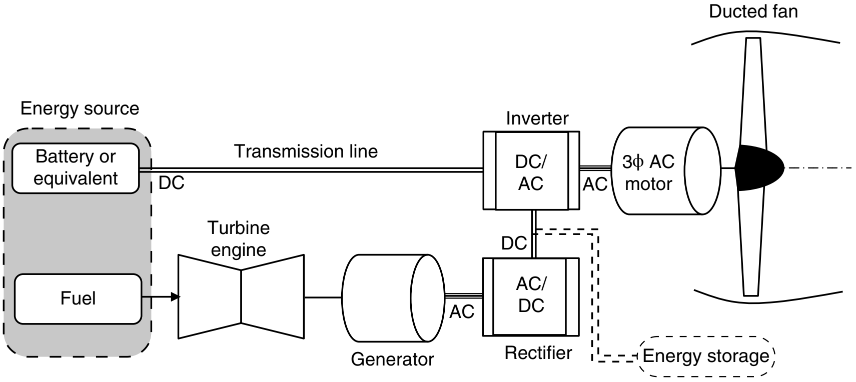

(a) Series hybrid-electric architecture with optional energy storage

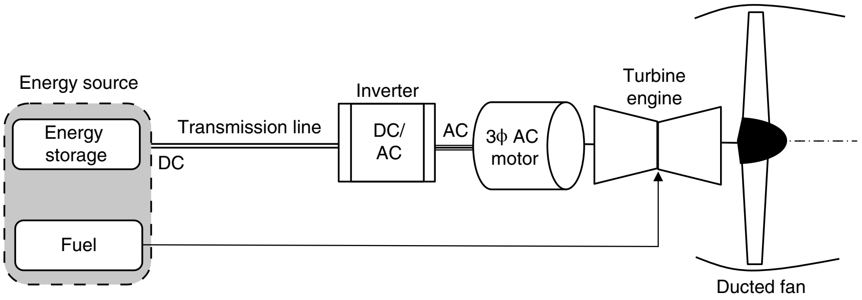

(b) Parallel hybrid-electric (used in Boeing SUGAR Volt –hFan; see Bradley-Droney 2011)

addition, since distributed propulsion is often envisioned as aft-mounted boundary layer ingestion (BLI) engines on a blended-wing-body (BWB) aircraft, shielding is a powerful strategy that is used to achieve quiet aircraft goals in hybrid-electric (or turboelectric) and distributed propulsion (DP) aircraft.

In hybrid-electric propulsion, the propulsor (ducted fan) may be operated by the gas turbine, using jet fuel, or by an electric motor that uses batteries or electric storage units, or combined Gas Turbine (GT) and electric motor as in parallel hybrid propulsion. Unique to this architecture is the need for variable-core nozzle in parallel hybrid-electric propulsion systems to accommodate the combined GT-electric motor operation and the transition between GT and the electric motor (23). The electric motor is connected to the LP spool via a gearbox. From taxi and take-off to climb, cruise, approach, and landing, the combined energy use and range is optimized by an electric power management hub.

"**Propulsive Fuselage**" is a hybrid-electric concept proposed by Bauhaus Luftfahrt in Germany for the Airbus A330-type, twin-aisle aircraft as a part of the Clean Sky 2 European Union-funded research program that is running from 2014 to 2024. Propulsive fuselage belongs to the broader ***Tailcone Thruster Propulsion*** concept (24). The goal is to mature promising technologies for an advanced airliner for entry into service (EIS) in 2030. The propulsive fuselage concept uses a third gas turbine engine that is embedded in the modified tailcone and powers an UHB fan in BLI configuration. This concept is shown in Figure 1.36.

■ FIGURE 1.36 "Propulsive Fuselage" hybrid-electric concept by Bauhaus Luftfahrt

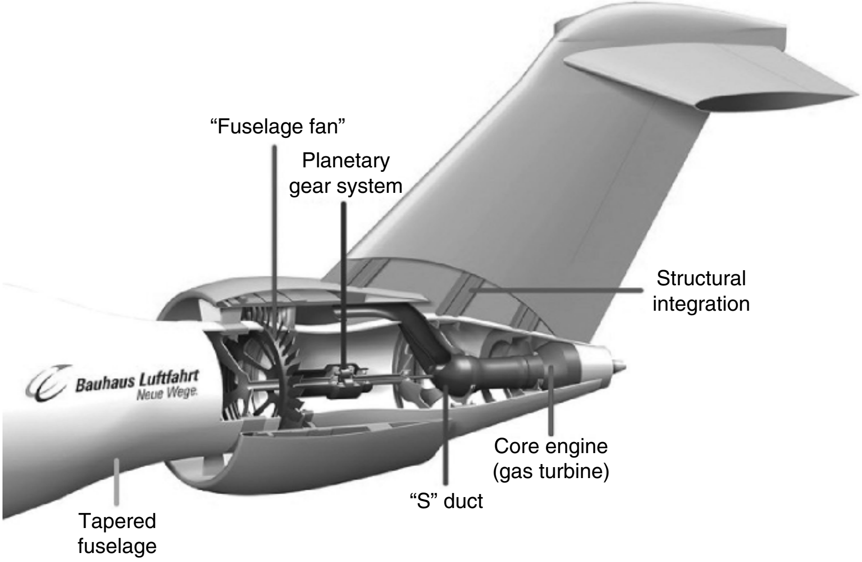

(a) "Propulsive fuselage" components

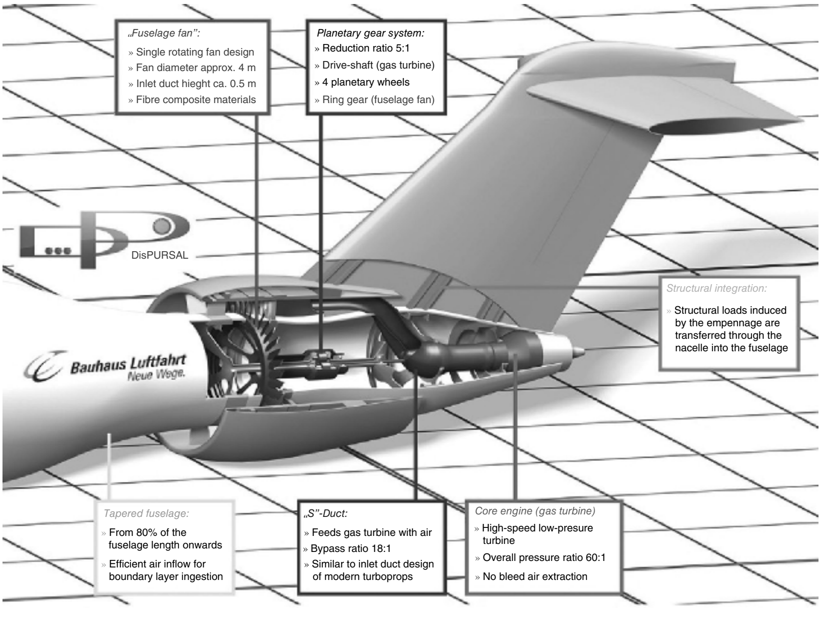

(b) Details of the propulsive fuselage, engine-airframe integration elements

Although in this configuration, the geared UHB is driven by the LPT, the electric motor-driven version is clearly the goal, which will be considered. Since the tail propulsor is in the aft fuselage-BLI position, it will reduce fuselage drag and engine noise. The preliminary studies showed an improvement in efficiency of 10%. This is a promising concept where BLI, geared-UHB/electric fan is used to reduce fuel burn and noise in an advanced hybrid-electric airliner.

The tailcone thruster concept was developed by NASA and is shown in Figure 1.37 (25, 26) for entry into service in 2035. The single-aisle turboelectric aircraft with aft-boundary layer propulsion, known as STARC-C ABL, uses the

■ FIGURE 1.37 Single-aisle turboelectric aircraft with aft-boundary layer ingestion propulsion system. (Source: From Welstead et al. (25))

(a) Tailcone thruster concept in STARC-C ABL aircraft

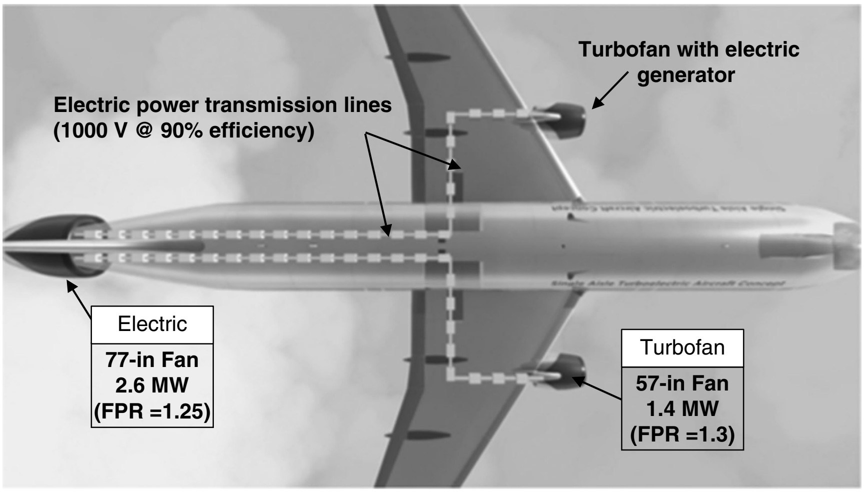

(b) Turboelectric propulsion concept used in STARC-C ABL aircraft with design mission of 3500 nm (From www1.grc.nasa.gov). Source: Glenn Research Center, NASA https://www1.grc.nasa.gov/

conventional tube-and-wing aircraft configuration with twin underwing turbofan engines that generate electric power for the aft-fuselage-mounted electric fan. The two underwing engines and the aft electric fan each provide one-third of the cruise thrust. The low-noise fan pressure ratio (FPR) for the two underwing engines was chosen at 1.3 and the electric BLI (low noise) fan had a pressure ratio of 1.25. The STARC-C ABL is shown (26) to provide between 7% and 12% reduction in block fuel (where 7% corresponds to the economic mission block fuel reduction for the 900 nm mission and the 12% is the design mission fuel burn reduction for the 3500 nm mission) as compared to conventional configurations. The electric transmission lines are nonsuperconducting, and the total electrical generation/transmission efficiency is assumed to be 90%. These are promising results for the EIS in 2035 that assumed a technology readiness level (TRL) of 6 for the key technologies by the year 2025. Since the aircraft in STARC-C ABL is the conventional tube-and-wing, the fuel burn reduction (of 7–12%) is almost entirely due to turboelectric propulsion with aft BLI fan. The fully integrated propulsion-airframe aircraft design with BLI, such as N3-X, contributes an additional 50% to block fuel reduction (27). In this context, 7–12% achieved in tube-and-wing STARC-C ABL is promising.

In advanced propulsion concepts, gas turbines are used as turbogenerators with the sole function of providing power to electric generators. Electric fans are driven by electric motors that receive their power from the electric generator. In this architecture, the power-producing unit (turbogenerator) is decoupled from the thrust-producing units (electric fans), as noted by Kim et al. (28). The new architecture allows for both units to operate at peak efficiency. The GT-power unit is a turboshaft core that drives an electric generator. The turboshaft core(s) may be placed in the aft fuselage or at the wing tips. Figure 1.38 shows the schematic drawing of a turboelectric propulsion system with an optional energy storage system (21, 22, 29). The electric components between the turbine and the fan compose the new elements of the *propulsive drivetrain* (shown as dashed line) in a turboelectric propulsion system. Power density and efficiency of the motor, generator, and power conversion units (rectifier, inverter); energy density of the batteries and other energy storage units; and the cooling system requirements and efficiency are all key performance parameters (KPP) in the propulsive drivetrain. The failure probability of each element and system reliability are critical to the viability of a turboelectric propulsion system. Fault-tolerant design and system redundancy are the main requirements of the hybrid and turboelectric propulsion system.

All-electric propulsion is solely powered by batteries or equivalent energy sources, as schematically shown in Figure 1.39. The carbon/environmental

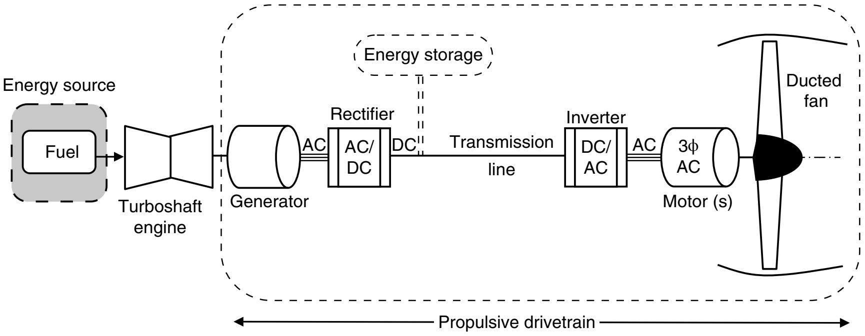

■ FIGURE 1.38 Schematic drawing of a turboelectric propulsion system driving a single ducted fan, with optional energy storage. (Source: Farokhi (11). Reproduced with permission of John Wiley & Sons)

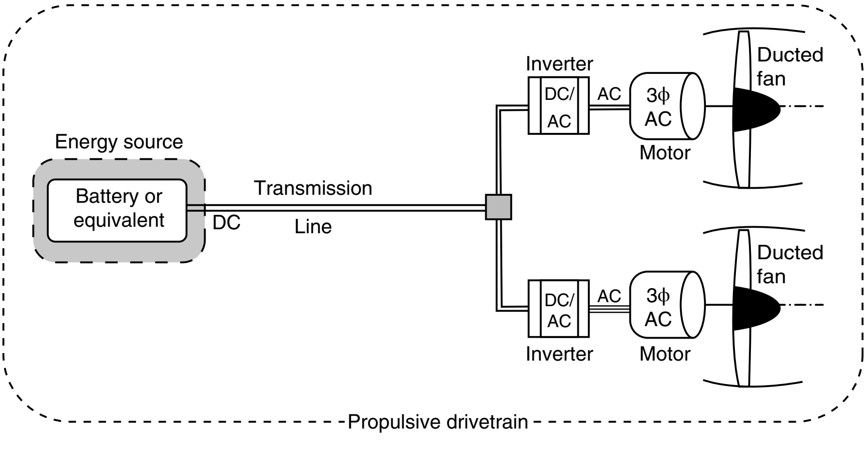

■ FIGURE 1.39 Schematic drawing of an all-electric propulsion system; here shown with two ducted fans. (Source: Farokhi (11). Reproduced with permission of John Wiley & Sons)

■ **FIGURE 1.40**
Zunum Aero hybrid-electric regional aircraft (12 seater) (Source: Zunum Aero)

footprint of electric propulsion is mainly in the type of charging systems used in charging the batteries. For example, using the coal-fired (fossil-fuel) based power grid or possibly renewable sources, such as solar or wind power, to charge the batteries impacts the carbon footprint. In addition, the environmental impact of mining for the minerals/metals used in batteries, for example, cadmium or lithium, needs to be accounted for in the environmental lifecycle assessment of electric propulsion.

A 12-seater hybrid-electric aircraft, shown in Figure 1.40, is proposed by Zunum Aero that targets the commuter, short-haul regional (700 mile) market. The concept aircraft uses lithium-ion batteries in the wings for supplementary power, especially at takeoff. In addition to propulsion batteries, cruise power is provided by a gas turbine engine that provides shaft power to a generator (30). A new turboshaft engine from Safran Helicopter, the Ardiden 3 engine with 1700–2000 shaft horsepower is envisioned to power electrical generator.

Figure 1.41 shows distributed turboelectric propulsion in an innovative design by Airbus. The technology uses:

- Decoupled power production and propulsion functions
- Coupled propulsion and aircraft aero functions
- Optional alternative source for energy storage

Figures 1.42 and 1.43 show the GT-based superconducting (SC) electric generator in the aft fuselage providing electric power through an SC-network of transmission lines.

■ **FIGURE 1.41** **Distributed turboelectric propulsion concept aircraft. (Source: Airbus)**

■ **FIGURE 1.42** **Turboelectric distributed propulsion concept. (Source: Airbus)**

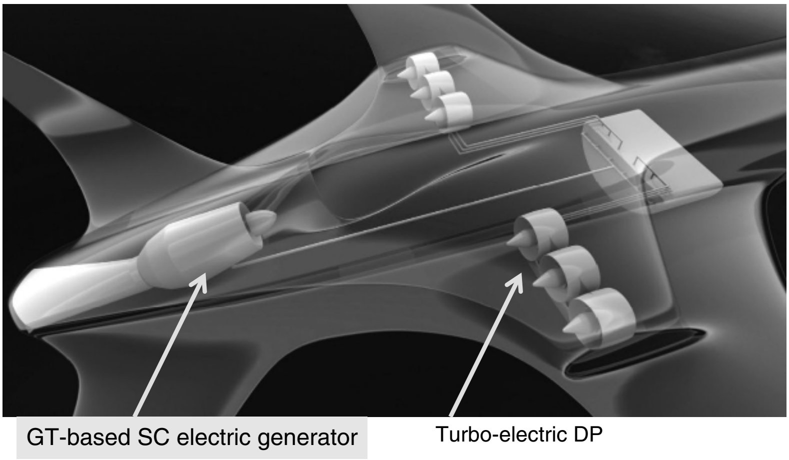

■ **FIGURE 1.43** **Superconducting network and electric power management. (Source: Airbus)**

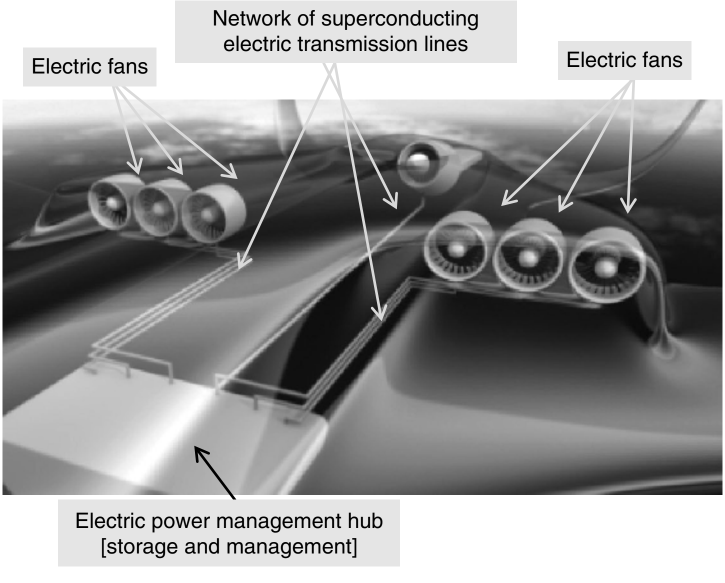

An example of turboelectric BLI-distributed propulsion (DP) is the NASA N3-X program. Due to extensive use of SC technology, N3-X uses LH_2 for direct cooling of the HTS network, SC motor, and SC generator. After its cooling cycle, hydrogen is then compressed and used for fuel in the turbogenerators. The fuel split is thus 10% hydrogen versus 90% jet fuel. The N3-X project goals are:

- $\sim$63% energy use reduction
- $\sim$90% NO_x reduction
- 32–64 EPNdB cumulative noise reduction as compared to the baseline Boeing 777-200 aircraft. Some of the design-driver characteristics of N3-X that present challenges are:
- Directional stability and control through differential thrust (for yaw trimming and active stability augmentation)
- Driving factors: safety and reliability
- Minimum weight penalty and volume requirements
- Acceptable system complexity
- Electrical system failure leading to thrust losses

Figure 1.44 shows the N3-X aircraft (courtesy of NASA). Tables 1.2 and 1.3 summarize the design point of N3-X as well as its mission specifications.

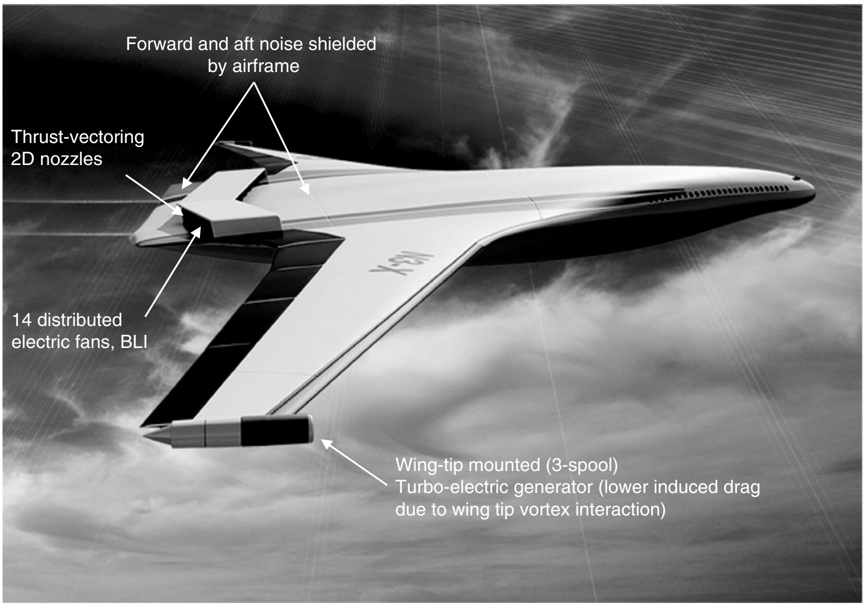

FIGURE 1.44
Distributed turboelectric propulsion. (Source: Courtesy of NASA)

TABLE 1.2
N3-X design point

Aerodynamic Design Point (ADP)	Mach	Altitude (ft)
Top-of-climb (TOC)	0.84	34,000

■ **TABLE 1.3**
Mission parameters

Parameters	**N3-X/MgB_2/LH_2 (Liquid Hydrogen Cooled)**
Range (nm)	7500
Payload (lbm)	118,100
Empty weight (lbm)	420,000
Block fuel weight (lbm)	76,171
Fan pressure ratio (FPR)	1.3
Net thrust (lbf)—installed	85,846 (RTO) and 33,405 (TOC)
TSFC (lbm/hr/lbf)—installed	0.2174 (RTO) and 0.3125 (TOC)
TSEC (BTU/s/lbf)—installed	1.1937 (RTO) and 1.727 (TOC)
Effective BPR, eBPR	36.1 (RTO) and 30.1 (TOC)
Air mass flow rate (lbm/s)	7823 (RTO) and 3696 (TOC)
Overall pressure ratio (OPR) (turboshaft engine)	57.3 (RTO) and 84.3 (TOC)

The data used in the tables and the figures related to N3-X are taken from Armstrong (29), Kim et al. (31), and Felder (22). Propulsion system parameters at rolling takeoff (RTO) and top-of-climb (TOC) are noted in Table 1.3.

Although the performance of the HTS turboelectric N3-X is produced here with MgB_2 (magnesium di-boride) superconductor, the choice of other SC materials and the cooling system is still a subject of research and could produce improvements in system weight and performance. For additional discussion, see Farokhi (11).

1.5 New Vehicle Technologies

Siemens, Airbus, and Rolls-Royce collaborated on developing a single-aisle commercial aircraft powered by a serial hybrid-electric propulsion system (HEPS). The near-term flight demonstrator was called E-Fan X (see Figure 1.45). The 2-MW electric motor and its power electronics control unit, including inverter, AC/DC converter, and the power distribution system, were developed by Siemens. Rolls-Royce was responsible for the turboshaft engine, 2 MW generator, and power electronics. Airbus was responsible for the overall system integration. The testbed aircraft was a BAe 146, which is a short-haul, regional airliner. This program, that is, E-Fan X, was canceled in April 2020. In September 2020, Airbus unveiled three new conceptual designs for their *zero-emission* hydrogen-hybrid commercial aircraft, dubbed as *ZEROe* (see Airbus website). The three Airbus commercial aviation concepts are centered around a twin turbofan, a twin turboprop, and a twin turbofan-powered, blended wing-body aircraft. These *ZEROe* aircraft use liquid hydrogen as fuel in their gas turbine engines as well as using hydrogen fuel cells to produce electric power. Airbus envisions an EIS of 2035.

The NASA X-57 aircraft, called *Maxwell*, is an all-electric distributed propulsion flight demonstrator with the goal of achieving an 80% reduction in energy

FIGURE 1.45 Modified BAe 146 aircraft used as hybrid-electric flight demonstrator. (Source: Airbus)

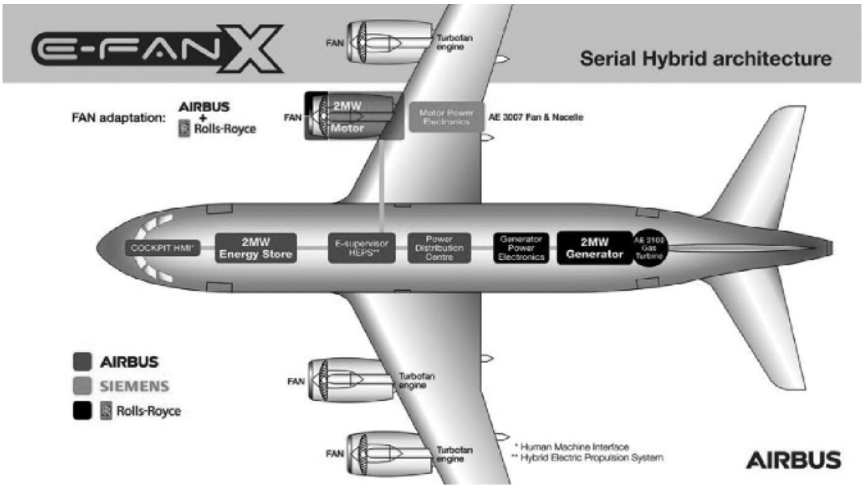

FIGURE 1.46 NASA X-57 all-electric distributed propulsion flight demonstrator. (Source: Courtesy of NASA)

consumption. The 12-wing-leading-edge mounted high-lift electric motors power 12-folding propellers and there are two larger wing tip electric cruise motors, as depicted in Figure 1.46. At TOC, the high-lift motors deactivate and their five folding propellers fold into the nacelle to mitigate drag rise during cruise. The X-57 is modified from the baseline Italian Tecnam P2006T aircraft. This program was launched in 2014 by the SCEPTOR (Scalable Convergent Electric Propulsion Technology and Operations Research) project at NASA. The final version of X-57 (i.e. Modification 4 in the program) will feature a high-aspect ratio wing with integral high-lift motors. Electric motors at Maxwell use rechargeable lithium-ion batteries that weigh 860 lb and offer 69.1 kWh of energy, of which 47 kWh is

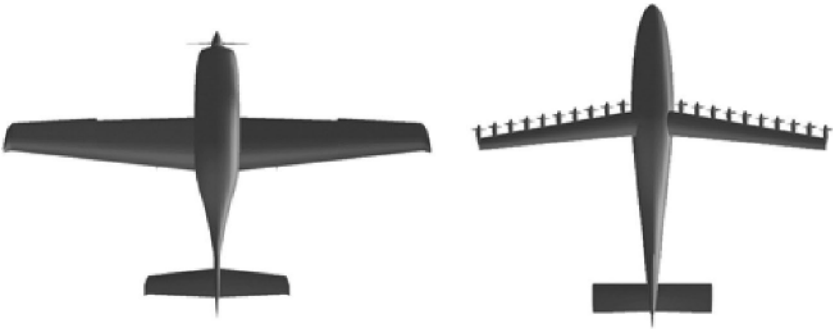

■ FIGURE 1.47
Cirrus SR22 and LEAPTech: a comparison

■ TABLE 1.4
Comparison of the Cirrus SR22 with the LEAPTech aircraft

	Cirrus SR22	LEAPTech
Seating capacity	4	4
Gross weight	3400 lbf	3000 lbf
Wing area	145 ft^2	55.1 ft^2
Wingspan	38.3 ft	31.0 ft
Aspect ratio	10.1	17.4
Wing loading	23.5 lbf/ft^2	54.4 lbf/ft^2
Cruise speed	211 mph	200 mph
Cruise C_L (12,000 ft)	0.30	0.77

usable. The cruise motors are 60 kW, and the 12 high-lift motors are 10.5 kW machines. The electric motors are air cooled. For more details on X-57, see Gibbs (32) or Warwick and Norris (33). The X-57 technology demonstrator program ended in June 2023.

Electric propulsion offers new aircraft design capabilities that are not possible in either conventional gas turbine-powered or reciprocating aircraft (34–36). The comparison between Cirrus SR22 and leading-edge asynchronous propellers technology (LEAPTech) aircraft is shown in Figure 1.47 and Table 1.4. LEAPTech aircraft have a 72% higher aspect ratio, wing loading which is 131%, and lift coefficient at cruise which is 157% higher than SR22. The wetted area of the LEAPTech wing is 62% less than the SR22 aircraft wing.

There are other exciting new vehicles on the drawing board for many different missions at many different speeds, for example, low-boom flight demonstrator and the hypersonic cruise missile. The interest in uninhabited aerial vehicles (UAVs) has also grown and prompted new configurations such as the Northrop–Grumman X-47 “Pegasus,” the tailless agility aircraft X-36 from Boeing, the X-45A unmanned combat air vehicle (UCAV), or the X-48 using blended wing-body technology. NASA’s interest in hypersonic flight and scramjet propulsion has prompted the X-43 series of technology demonstrator vehicles. Some of these and other aircraft are shown in Figure 1.48. All technology demonstrator aircraft are indeed *pathfinders*.

■ **FIGURE 1.48** **Uninhabited aerial vehicles and NASA technology demonstrators. (Source: Boeing and NASA. Reproduced with permission)**

Boeing X-45A UCAV

Boeing X-36

NASA X43-A Mach 10 airbreathing technology demonstrator

Boeing X-48B

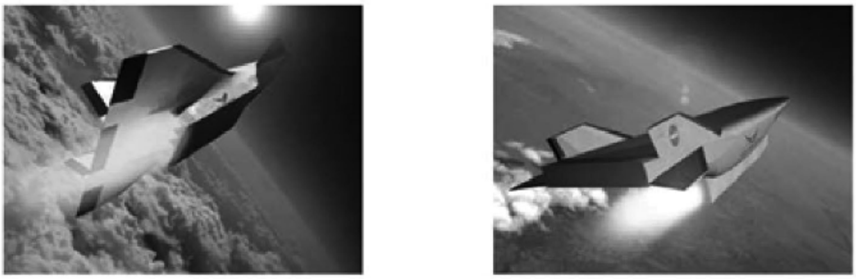

NASA X43-B technology demonstrator

NASA X43-C technology demonstrator

Boeing X-48A

1.6 Summary

There are exciting developments in aerospace propulsion system and sustainable aviation:

- Physics-based computer simulation/design is the game changer.
- Advanced composite materials for lightweight and high-temperature applications.
- Digital fabrication and manufacturing will take unprecedented precision from the nanoscale upward, including 3D printing and digital assembly.
- Additive manufacturing goes to space onboard the ISS.

- Exciting new vehicles on the horizon from low speed to hypersonic.
- Sustainable aviation seeks other energy sources than fossil fuels, for example, renewable jet fuels and electric energy sources.
- Sustainable aviation fuels (SAF) as well as cryogenic fuels LH_2 and LNG will power sustainable aviation.
- Hybrid and electric propulsion hold the promise of reduced GHG emissions.
- NASA X-planes are back! Use the excitement to attract a new generation of STEM students and future aero-enthusiasts and astronauts.
- Harnessing unsteadiness as a means of propulsion will open a new chapter in aircraft propulsion.
- Synergetic airbreathing rocket engine (SABRE) technology is promising.
- Advanced GT engines, such as high-efficiency, low-emission, quiet engines, for example, PW1000G and geared UHB turbofan engine powers large transport aircraft.
- RBCC propulsion: from takeoff to orbit!
- New launch vehicles and missions for hypersonic aircraft and space exploration.
- NASA to return humans to the Moon: crewed mission is now planned for 2026.
- The next frontier: manned mission to Mars will begin by 2030.
- Space tourism from suborbital flights, to orbit, to the Moon, and beyond are gaining popularity.
- The United States, Europe, China, Russia, Japan, and India are all active in commercial space race!
- Finally, emerging technologies in manufacturing, such as AI, ML, DT, and XR are the imminent tools of the new frontier.

1.7 Roadmap for the Fourth Edition

Engine thrust and performance parameters are discussed in Chapter 2, where rigorous derivation of uninstalled thrust and installation effects are presented. Gas turbine engine cycle analysis, for both ideal and real components, is studied in Chapter 3, including a section on UHB engines. We address sustainable propulsion systems through innovative cycles that involve multiple combustion chambers and multiple fuels, as well as cycles that use intercooler and recuperator. Advanced turbine technologies, such as tip clearance control, variable-area turbine (VAT) architecture, and turbine cooling, are presented in Chapter 3. Aircraft engine inlets and nozzles, over a wide speed range, are analyzed in Chapter 4. An expanded section on aircraft noise in landing-takeoff (LTO) cycle including airframe and engine noise, jet noise, and various mitigation methods such as Chevron Nozzle is presented in Chapter 4. With rising interest in supersonic business jets, as well as commercial transport, sonic boom generation, and its mitigation for overland flight is also addressed in Chapter 4. The principles of combustion are detailed in Chapter 5. The specific characteristics of the primary and afterburners, as in flameholding, are discussed in the same chapter. As an element of sustainable aviation, that is, *Sustainable Aviation Fuel* (SAF) from renewable sources and cryogenic fuels such as LH_2 and LNG are presented in Chapter 5. The turbomachinery principles and their application to axial-flow compressor, centrifugal compressor, and the axial-flow turbine are extensively derived and discussed in Chapters 6–8. Additional design guidelines are added to turbomachinery chapters. Chapter 9 aims to integrate all the gas turbine engine components into a unified system, from component matching to engine off-design analysis. This chapter also includes the principles of engine performance testing. Chapter 10 is a new chapter in the 4th edition dedicated to supersonic and hypersonic propulsion. The topics include flow control strategies, *Adaptive Cycle Engine* (ACE), conventional and supersonic combustion ramjets, and combined cycle propulsion systems. An overview of available computational and online resources and links related to propulsion is also assembled in a separate appendix. The online resources in the third edition are expanded to include gas tables for different ratios of specific heats, all the equations, and figures in the book. Finally, to reduce the page count in the fourth edition, the review of aerothermodynamics, unmanned aerial vehicle (UAV) engines, and some rocket propulsion sections are moved from print to *Online Resources*, which are available to our readers.

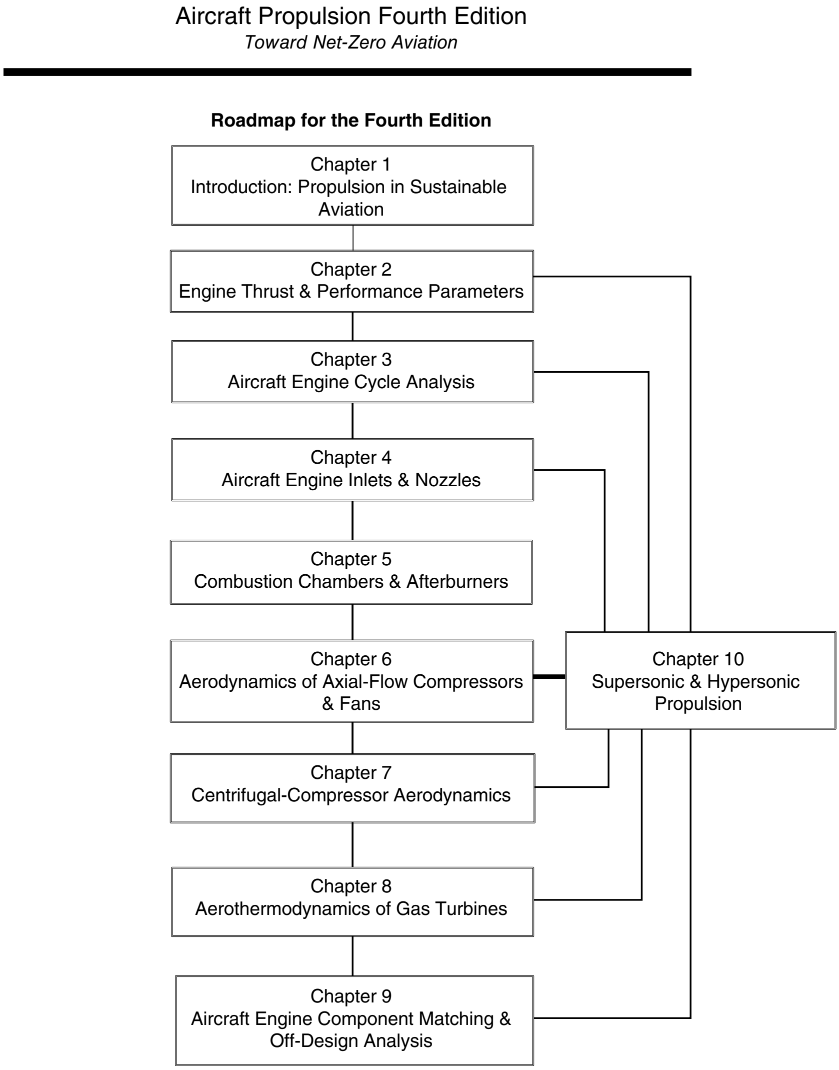

References

1. Meher-Homji, C.B., “The Development of Whittle Turbojet,” ASME Paper No. 97-GT-528, 1997.
2. Eckardt, D., *Jet Web—Connections in the Development History of Turbojet Engines 1920–1950*, Springer Verlag, Wiesbaden, Germany, 2022.
3. Meher-Homji, C.B., “The Development of Junkers Jumo 004B—The World’s First Production Turbojet,” ASME Paper No. 96-GT-457, 1996.
4. Dawson, V.P., *Engines, and Innovation: Lewis Laboratory and American Propulsion Technology*, NASA SP-4306, Washington, DC, 1991.
5. Wallace, L.E., *Flights of Discovery: Fifty Years at the NASA Dryden Flight Research Center*, National Aeronautics and Space Administration, Washington, DC, 1996.
6. NASA, “History Division’s Website,” http://history.nasa.gov/ (last accessed 16 November 2013).
7. NASA, http://www.nasa.gov/centers/dryden/news/FactSheets (last accessed 16 November 2013).
8. NASA, “Celebrating a Century of Flight,” NASA Publication SP-2002-09-511-HQ.
9. Brindley, B., “Additive Manufacturing,” Presentation at the Additive Manufacturing for Defense and Government Symposium, Washington, DC, 13–14 May 2015. https://ammo.ncms.org
10. Conner, B.P., Monagharan, G.P., Martof, A.N., Rodomsky, L.M., Rodomsky, C.M., Jordan, D.C., and Limperos, J.W., “Making Sense of 3-D Printing: Creating a Map of Additive Manufacturing Products and Services,” *Additive Manufacturing*, Vol. 1–4, pp. 64–76, October 2014, doi:https://doi.org/10.1016/j.addma.2014.08.005.
11. Farokhi, S., *Future Propulsion Systems and Energy Sources in Sustainable Propulsion*, John Wiley & Sons Ltd., Chichester, UK, 2020.
12. Fetterer, F., Knowles, K., Meier, W. and Savoie, M., “*Sea Ice Index, Version 2. National Snow and Ice Data Center*, Boulder, Colorado, 2016.
13. European Commission, *Future Transport Fuels: Report of the Expert Group*, Publications Office of the European Union, 2015.
14. Lee, D.S., Fahey, D.W., Forster, P.M., Newton, P.J., Wit, R.C.N., Lim, L.L., Owen, B., and Sausen, R., “Aviation and Global Climate Change in the 21st Century,” *Atmospheric Environment*, Vol. 43, pp. 3520–3537, 2009.
15. Sehra, A.K., and Shin, J., “Revolutionary Propulsion Systems for 21st Century Aviation,” NASA/TM-2003-212615, 2003.
16. Epstein, A.H., “Aeropropulsion for Commercial Aviation in the Twenty-First Century and Research Directions Needed,” *AIAA Journal*, Vol. 52, No. 5, pp. 901–911, May 2014.
17. Farokhi, S., “Pressure-Time History of Pylon-Wake (Signature) on a Pusher Propeller in Flight,” *AIAA Journal of Propulsion and Power*, Vol. 6, No. 6, pp. 758–768, November–December 1990.
18. Welch, G.E., Jones, S.M., and Paxson, D.E., “Wave Rotor-Enhanced Gas Turbine Engines,” NASA TM-106998, 1995.
19. Akbari, P., Nalim, M.R., and Müller, N., “A Review of Wave Rotor Technology and Recent Developments,” *Journal of Engineering for Gas Turbines and Power*, Vol. 128, No. 4, pp. 715–735, 2006.
20. Akbari, P., Szpynda, E., and Nalim, M.R., “Recent Developments in Wave Rotor Combustion Technology and Future Perspectives: A Progress Review,” AIAA Paper Number 2007-5055, presented at the 43rd AIAA/ASME/SAE/ASEE Joint Propulsion Conference and Exhibit, Cincinnati, OH, 6–11 July 2007.
21. Del Rosario, R., “A Future with Hybrid Electric Propulsion Systems: A NASA Perspective,” Turbine Engine Technology Symposium, Strategic Visions Workshop, Dayton, OH, September 2014.
22. Felder, J.L., “NASA N3-X with Turboelectric Distributed Propulsion,” Presentation at the Institution of Mechanical Engineers, London, UK, 17–18 November 2014.
23. Bradley, M.K., and Droney, C.K., “Subsonic Ultra Green Aircraft Research: Phase I Final Report,” NASA/CR-2011-216847, 2011.
24. Dyson, R., “NASA Hybrid Electric Aircraft Propulsion,” Presentation at the NIEA Biomimicry Summit, October 2017.
25. Welstead, J., Felder, J., Guynn, M., Haller, B., Tong, M., Jones, S., Ordaz, I., Quinlan, J., and Mason, B., “Overview of the NASA STARC-C ABL (Rev. B): Advanced Concept,” https://ntrs.nasa.gov/archive/nasa/casi.ntrs.nasa.gov/20170005612.pdf
26. Welstead, J.R., and Felder, J.L., “Conceptual Design of a Single-Aisle Turboelectric Commercial Transport with Fuselage Boundary Layer Ingestion,” AIAA Paper No. 2016-1027 Presented at the AIAA SciTech Conference, January 2016.
27. Jansen, R.H., Bowman, C., and Jankovsky, A., “Sizing Power Components of an Electrically Driven Tailcone Thruster and a Range Extender,” Presented at the 16th AIAA Aviation Technology, Integration, and Operations Conference, June 2016.
28. Kim, H.D., Brown, G.V., and Felder, J.L., “Distributed Turboelectric Propulsion for Hybrid Wing Body Aircraft,” Paper Presented at the 2008 International Power Lift Conference, London, England, July 2008.
29. Armstrong, M., “Superconducting Turboelectric Distributed Aircraft Propulsion,” Presentation at the Cryogenic Engineering Conference, July 2015.

30. Knapp, M., and Said, W., “Zunum Aero’s Hybrid-Electric Airplane Aims to Rejuvenate Regional Travel,” *IEEE Spectrum*, 26 April 2018.
31. Kim, H.D., Felder, J.L., Tong, M.T., and Armstrong, M., “Revolutionary Aeropropulsion Concept for Sustainable Aviation: Turboelectric Distributed Propulsion,” ISABE Conference, Paper Number 2013-1719, 2013.
32. Gibbs, Y., “NASA Armstrong Fact Sheet: NASA X-57 Maxwell,” 27 August 2018, https://www.nasa.gov/centers/armstrong/news/FactSheets/FS-109.html
33. Warwick, G., and Norris, G., “NASA Shares Hard Lessons as All-Electric X-57 Moves Forward,” *Aviation Week & Space Technology*, 5 June 2018.
34. Gohardani, A.S., “A Synergistic Glance at the Prospects of Distributed Propulsion Technology and the Electric Aircraft Concept for Future Unmanned Air Vehicles and Commercial/Military Aviation,” *Progress in Aerospace Sciences*, Vol. 57, pp. 25–70, February 2013.
35. Moore, M.D., and Fredericks, W.J., “Misconceptions of Electric Propulsion Aircraft and their Emergent Aviation Markets,” 52nd Aerospace Sciences Meeting, AIAA SciTech Forum, AIAA Paper Number 2014-0535, 2014.
36. Moore, M.D., Fredericks, W.J., Borer, N.K., Stoll, A. M., and Bevirt, J., “Drag Reduction Through Distributed Electric Propulsion,” Aviation Technology, Integration, and Operations Conference, Atlanta, GA, 2014.

Suggested Additional Reading

Airbus Press Release 2017, “Airbus, Rolls-Royce and Siemens Team Up for Electric Future Partnership Launches E-Fan X Hybrid-Electric Flight Demonstrator,” 28 November 2017. https://www.airbus.com/newsroom/press-releases/en/2017/11/

Airbus’ Website on ZEROe Concept Aircraft Press Release, https://www.airbus.com/newsroom/press-releases/en/2020/09/airbus-reveals-new-zeroemission-concept-aircraft.html (last accessed 23 September 2020).

Bauhaus Luftfahrt, “Propulsive Fuselage Concept,” https://www.bauhaus-luftfahrt.net/en/topthema/propulsive-fuselage/

Bullis, K., “A More Efficient Jet Engine Is Made from Lighter Parts, Some 3-D Printed,” *MIT Technology Review*, May 2013.

Devola, E., “Sustainable Manufacturing; Re-Imagining Production,” *SAE International, Tech Briefs*, Vol. 48, No. 1, pp. 17, January 2024.

Environmental Protection Agency, “Control of Air Pollution from Aircraft and Aircraft Engines,” Federal Register, Vol. 47, No. 251, 1982.

Environmental Protection Agency, “Control of Air Pollution from Aircraft and Aircraft Engines,” Federal Register, Vol. 38, No. 136, 1973.

Environmental Protection Agency, “Control of Air Pollution from Aircraft and Aircraft Engines,” Federal Register, Vol. 43, No. 58, 1978.

Environmental Protection Agency, “Control of Air Pollution from Aircraft and Aircraft Engines,” Federal Register, Vol. 47, No. 251, 1982.

Environmental Protection Agency, “Inventory of US GHG Emissions and Sinks,” Annual Report, 2022.

Federal Aviation Administration, “Aviation & Emissions: A Primer”, Washington, DC, 2005.

GE Aviation Website, www.geaviation.com (last accessed 3 October 2020).

Hooper, S., “Artificial Intelligence; How Cloud Technology and AI Drives a More Productive Future,” *SAE International, Tech Briefs*, Vol. 48, No. 1, pp. 12, January 2024.

Hooper, S., Kauffman, R., Klotz, W., Worth, J., and Devola, E. “Emerging Technologies in Manufacturing,” *SAE International Tech Briefs*, Vol. 48, No. 1, pp. 11–17, January 2024.

Kauffman, R., “6G; Will It Trigger a Manufacturing Revolution?” *SAE International, Tech Briefs*, Vol. 48, No. 1, pp. 13, January 2024.

Klotz, W., “Digital Twins; The Next Steps,” *SAE International, Tech Briefs*, Vol. 48, No. 1, pp. 14, January 2024.

Made In Space Website, https://madeinspace.us (last accessed 7 October 2020).

Mechanical Engineering Magazine, “Milestone for 3D-Printed Jet Engine,” *Mechanical Engineering Magazine*, p. 22, June/July 2024.

Meher-Homji, C.B., “Pioneering Turbojet Developments of Dr. Hans von Ohain—From HeS 01 to HeS 011,” ASME Paper No. 99-GT-228, 1999.

NASA, “NASA, Boeing, Provide a Peek at What the X-66A Will Look Like,” https://www.nasa.gov/image-article/nasa-boeing-provide-a-peek-at-what-the-x-66a-will-look-like/

National Institute of Standards and Technology (NIST) Website, www.nist.gov/publications (last accessed 3 October 2020).

NOAA Website, www.esrl.noaa.gov/gmd/ccgg/trends/

Northrop Grumman Website, www.nothropgrumman.com (last accessed 3 October 2020).

Pratt & Whitney Website, www.prattwhitney.com (last accessed 3 October 2020).

The US Patent, "The U.S. Patent 4,072,008 (1978) is granted on Variable Area Bypass Injector System," 7 February 1978.

The Website of Reaction Engines Ltd, www.reactionengines.co.uk

Worth, J., "Extended Reality; Immersing into the Future of Manufacturing," *SAE International, Tech Briefs*, Vol. 48, No. 1, pp. 15–16, January 2024.

Zunum Aero's Website, https://zunum.aero.

Problems

1.1 The Carnot cycle sets the limit on thermal efficiency of a heat engine operating between two temperature limits. Show that ideal Carnot efficiency is:

What is the thermal efficiency if $T_1 = 288$ K and $T_2 = 2000$ K?

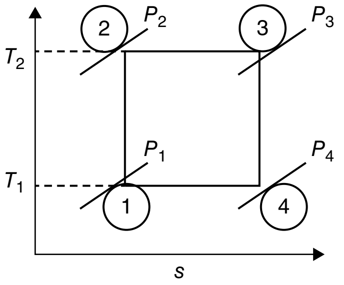

■ **FIGURE P1.1**

1.2 The ideal Brayton cycle operates between two pressure limits as shown. It is the model of an airbreathing jet engine, such as a turbojet or ramjet engine. Show that the ideal Brayton cycle thermal efficiency is:

$$\eta_{\text{th}} = 1 - \frac{T_1}{T_2}$$

What is the thermal efficiency of the Brayton that has $T_1 = 288$ K and $T_2 = 864$ K? Note that maximum cycle temperature T_3 has no effect on cycle thermal efficiency.

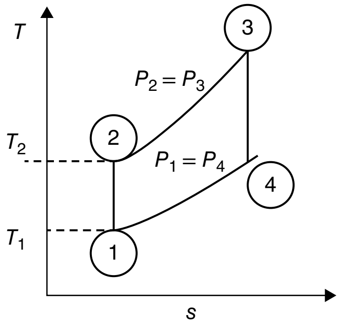

■ **FIGURE P1.2**

1.3 The Humphrey cycle operates a constant-volume combustor instead of a constant-pressure cycle like the Brayton cycle. Show that:

$$\eta_{\text{th}} = 1 - \gamma \frac{T_1}{T_2}\left[\left(\frac{T_3}{T_2}\right)^{\frac{1}{\gamma}} - 1\right] \Big/ \left[\frac{T_3}{T_2} - 1\right]$$

is the thermal efficiency of an ideal Humphrey cycle (as shown).

Let us use the same T_1 as in Problems 1.1 and 1.2, that is, $T_1 = 288$ K. Let us use the same temperature T_2 as in Problem 1.2, that is, $T_2 = 864$ K.

Finally, let us use the same maximum cycle temperature as in Carnot (Problem 1.1), that is, $T_{\max} = 2000$ K. With the ratio of specific heats $\gamma = 1.4$, calculate the thermal efficiency of the Humphrey cycle. Compare the answer with Brayton cycle efficiency.

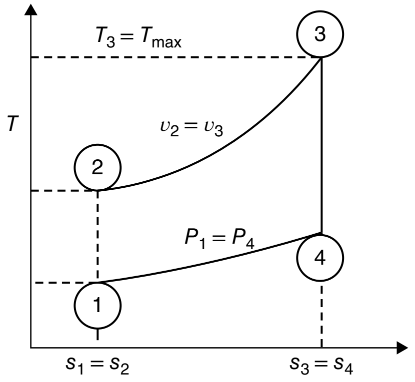

■ **FIGURE P1.3**

1.4 The rotor of a millimeter-scale gas turbine engine has a radius of 1 mm. It must reach a tip or rim speed of nearly the speed of sound for an effective compression. Assuming that the speed of sound is 340 m/s, calculate the rotor rotational speed in revolutions per minute (rpm).

1.5 Specific fuel consumption (sfc) projects the fuel economy of an engine, that is, it measures the fuel flow rate (say in pound-mass per hour or g/s) that leads to a production of a unit thrust (say 1 pound-force or 1

Newton). Two sets of numbers are copied from Table 1.1 (from EJ200 specification), which are:

sfc (max. power)	0.81 lbm/h/lbf
sfc w. AB	1.75 lbm/h/lbf
Thrust (SL)	13,500 lbf
Thrust w. AB	20,250–22,250 lbf

First note that afterburner (AB) uses more than double the fuel consumption while boosting the thrust by only ~50%. This explains the sparse use of an afterburner in aircraft missions. Now to quantify, calculate the amount of additional fuel burned in 30 min of afterburner use (producing 21,000 lbf thrust) as compared with 30 min of no afterburner use (producing 13,500 lbf thrust).